Bulletin of the Seismological Society of America, Vol. 98, No. 4, pp. 1983–2003, August 2008, doi: 10.1785/0120070277

Comparisons of Shear-Wave Slowness in the Santa Clara Valley, California, Using Blind Interpretations of Data from Invasive and Noninvasive Methods

by David M. Boore and Michael W. Asten

Abstract Many groups contributed to a blind interpretation exercise for the determination of shear-wave slowness beneath the Santa Clara Valley. The methods included invasive methods in deep boreholes as well as noninvasive methods using active and passive sources, at six sites within the valley (with most investigations being conducted at a pair of closely spaced sites near the center of the valley). Although significant variability exists between the models, the slownesses from the various methods are similar enough that linear site amplifications estimated in several ways are generally within 20% of one another. The methods were able to derive slownesses that increase systematically with distance from the valley edge, corresponding to a tendency for the sites to be underlain by finer-grained materials away from the valley edge. This variation is in agreement with measurements made in the boreholes at the sites.

Introduction

Shear-wave slownesses (where slowness is the inverse of velocity) within several hundred meters of the Earth's surface are important in specifying earthquake ground motions for engineering design. Not only are the shear-wave slownesses used to classify sites in modern building codes, but they are also used in site-specific studies of particularly significant structures. Many are the methods for estimating subsurface shear-wave slownesses, but few are the blind comparisons of the slownesses resulting from independent interpretations of multiple measurements using different methods at a single site—what we call a blind interpretation exercise (e.g., Brown *et al.*, 2002; Stephenson, Louie, *et al.*, 2005; Cornou *et al.*, 2007). The word blind is important here and means that the measurements and interpretations were performed independently of one another. We present here the results of one blind interpretation exercise conducted at six sites in the Santa Clara Valley, California (Fig. 1). Boreholes were drilled to several hundred meters by the Santa Clara Water District at these sites (Hanson *et al.*, 2002), and in a collaborative study with a number of U.S. Geological Survey (USGS) researchers, the holes were made available for downhole logging (Newhouse *et al.*, 2004). Stephen Hartzell of the USGS realized that these boreholes presented an opportunity for assessing the strengths and weaknesses of the various measurement and interpretation methods, and he and USGS scientists Jack Boatwright and Carl Wentworth recommended that one of the borehole sites, in the city of San Jose, California, be used for the blind interpretation exercise: the site had good access and adequate space for conducting measurements. This site is the Coyote Creek Outdoor Classroom (CCOC), adjacent to William Street Park (WSP). The borehole was at CCOC, but many of the measurements were at WSP, 200 m from CCOC. The first author of this article (D. M. B.) took on the job of coordinating the exercise. He persuaded several teams to make measurements, helped with the local logistics, collected the results, and organized and conducted an international workshop in May 2004, at which the participants in the exercise gathered in Menlo Park, California, to describe their measurements and interpretations, and to see the results of the comparisons of the various methods for the first time. An important part of the process is that borehole geophysical and geological data were not provided to participants until interpretation reports were received by D. M. B. The second author of this article (M. W. A.), who was one of the participants in the exercise, took the lead in preparing an Open-File Report describing the results of that workshop (Asten and Boore, 2005a).

A number of the investigator teams also made measurements and provided slowness models at five other boreholes (results from some of these measurements are discussed in Stephenson, Louie, *et al.* [2005]). In this article, we present results for all of the sites, with a focus on

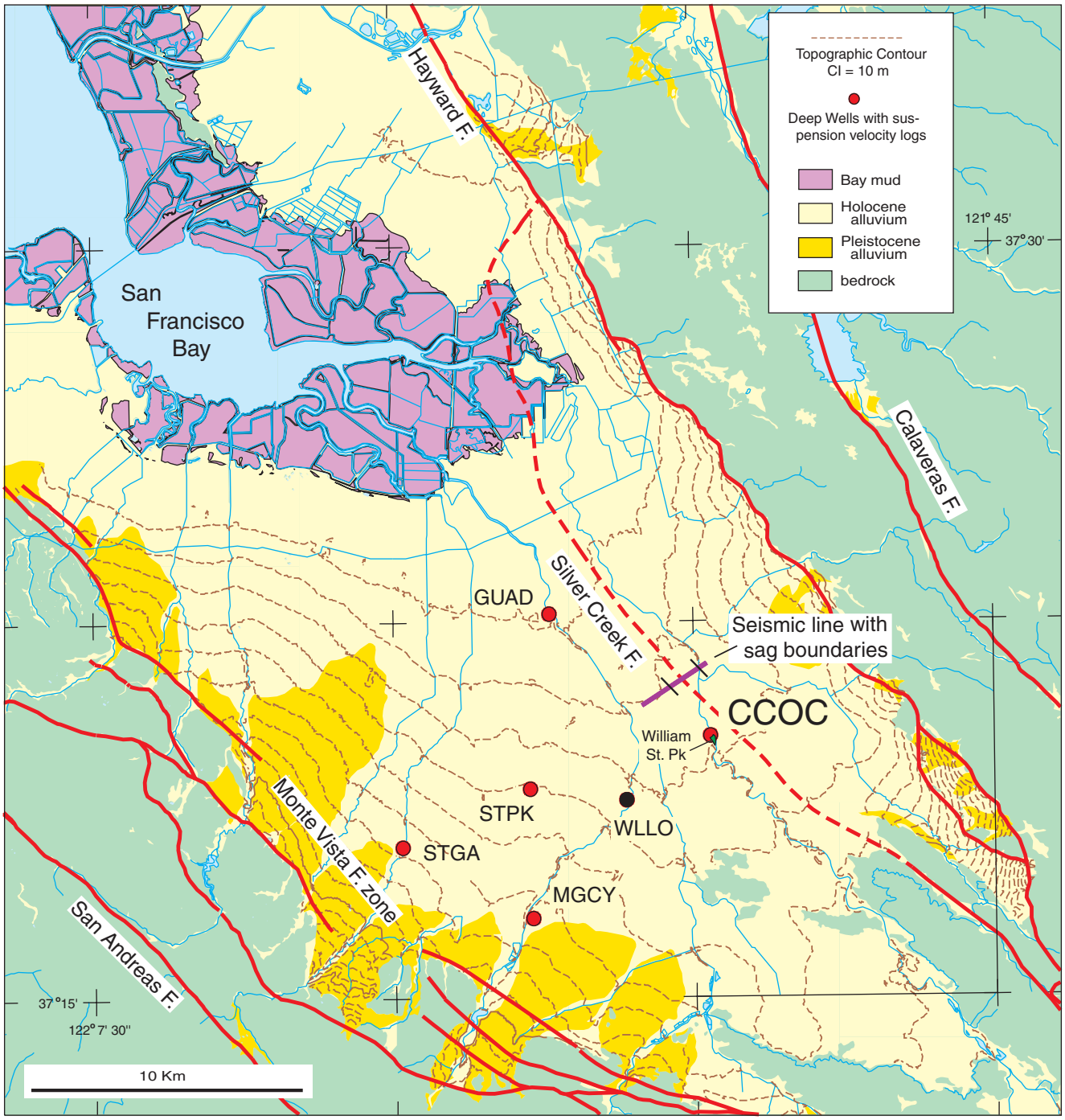

Figure 1. Location map of the blind interpretation sites. The labeled circles are the locations of boreholes; all but WLLO were logged using the SPSVL method. The coordinates of CCOC are 21.86835° E, 37.33702° N (North American Datum of 1927 [NAD27]; from Wentworth and Tinsley, 2005).

the CCOC/WSP site. Our article not only illustrates the variability in slowness at a single site resulting from independent measurements and interpretations, but it also finds a systematic increase in slowness with increasing distance from the valley edge, consistent with geologic considerations (coarse-grained alluvial sediments or older sediments near the valley edge and fine-grained fluvial sediments near the valley center). The most important result of our study may be that the variability in the slowness models is small enough that predictions of linear site amplifications based on average slownesses are generally within 20% of one another.

We use slowness as the material parameter of interest rather than velocity, for reasons discussed in Brown *et al.* (2002) and Boore and Thompson (2007). In brief, slowness (which is the inverse of velocity) is more directly related to site amplification than velocity and is a more sensitive indicator of variability near the surface. We use S_S to indicate shear-wave slowness (and, when used, V_S for shear-wave velocity).

Geologic Setting

The Santa Clara Valley is a subsiding trough filled by Quaternary sediments eroded from the surrounding mountains. The surficial geology and a cross section of the valley are shown in Figures 1 and 2. An excellent discussion of the geology and the implications for variability from site to site is given in Wentworth and Tinsley (2005). Tectonic subsidence, sea-level changes related to glaciation, and climate changes have produced a number of cycles of sedimentation. These cycles are characterized by alterations of fine- and coarse-grained sediments in the Quaternary section. In general, the sediments are approximately flat lying (with a gradient on the order of 2 m/km), with little variability over distances of several hundred meters (at least for sites near the center of the valley; Wentworth and Tinsley, 2005). On the other hand, there is a clear tendency for the slowness to depths of least 300 m to increase with increasing distance from the edge of the valley; this is shown in Figure 3, in which slownesses from suspension *P*- and *S*-wave (PS) velocity logs (SPSVL) averaged over 5-m depth intervals are plotted against depth (the SPSVL models were obtained by R. A. Steller of GeoVision using an Oyo suspension logging system, under contract to the USGS). The sediments were deposited unconformably on Tertiary Miocene rocks in the west part of the valley and on Cretaceous/Jurassic Franciscan and Great Valley formation rocks near the center of the valley (Fig. 2). These rocks form the effective bedrock for the sites, and the top surface of these rocks ranges in depth from about 240 to 410 m at the sites of interest in this study, as estimated from gravity studies, borehole measurements, and seismic reflection and refraction studies (e.g., Wentworth and Tinsley, 2005; Catchings *et al.*, 2006; C. Wentworth, personal comm., 2006).

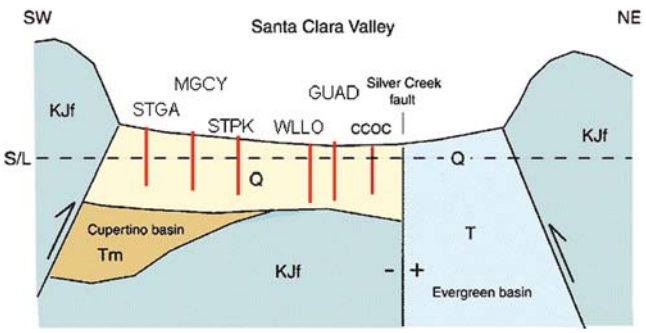

Figure 2. Schematic cross section through the Santa Clara Valley, approximately along the line from MGCY to CCOC (Fig. 1). The Quaternary sediments at sites MGCY, STGA, and probably STPK are underlain by Tertiary sedimentary rock (denoted as Tm), and at WLLO, CCOC, and GUAD the Quaternary sediments are underlain by the Franciscan assemblage of Cretaceous and Jurassic age (denoted as KJf). *S*/*L* indicates sea level. The drawing is not to scale, and there is a large vertical exaggeration (the depth to KJf at CCOC is 410 m); from Wentworth and Tinsley, 2005.

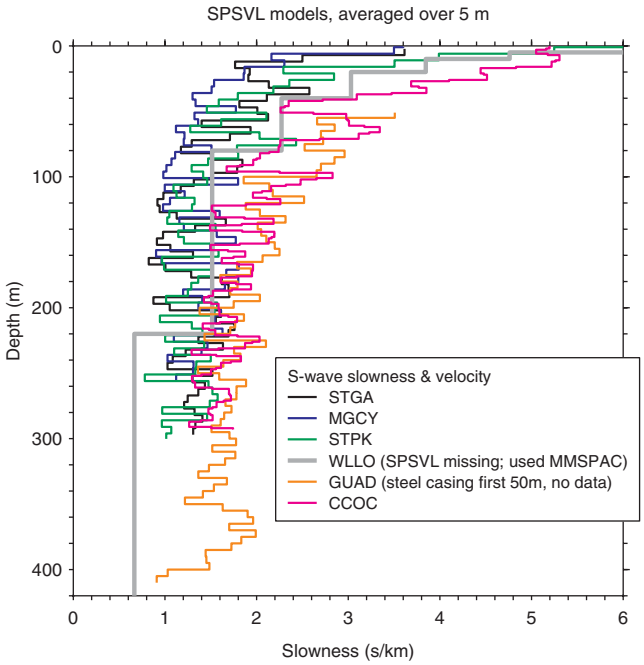

Figure 3. Slowness from SPSVL interpretations for all sites (because no SPSVL measurements were done at WLLO, we show the inversion results of the second author) ordered according to distance from the valley edge. Note that the slowness generally increases laterally with increasing distance from the valley edge.

Methods for Determining Subsurface Slowness

We classify methods for estimating slowness into two major groups: invasive and noninvasive (Table 1). Within each group, the methods can be further divided into groups using active sources (such as electromechanical vibrators or impact sources) and passive sources (such as ambient noise) to generate the waves from which the slowness models are derived; some methods combine measurements from active and passive sources. We were fortunate to have representatives of most of the methods given in Table 1. The specific methods applied to the sites in our study are given in Table 2. All of these methods were applied to the CCOC/WSP sites, and a subset of the methods was applied at the other sites. We make no attempt here to discuss the measurement and interpretation methods; reviews of these can be found in Asten and Boore (2005b), Stephenson, Louie, *et al.* (2005), Asten (2006), and Boore (2006), and in the selected references given in Table 2.

In this article, we present results only for shear-wave slowness. We do this for two reasons: (1) because most of

Table 1
General Classification of Methods for Obtaining Near-Surface Slowness Models

Invasive Methods	Noninvasive Methods
• Surface source – Receiver in borehole – Receiver in cone penetrometer • Downhole source – Suspension PS logger – Crosshole	• Single station (H/V) • Multiple stations – Active sources (linear spread of receivers) Reflection/Refraction SASW MASW – Passive sources (2D array of receivers) FK SPAC ReMi (receivers in line) – Combined active and passive

See Table 2 for meaning of abbreviations; from Boore, 2006.

the noninvasive methods based their compressional-wave slowness models on assumptions about Poisson's ratio or the depth to the saturated layer rather than actual measurements of compressional waves and (2) because shear-wave slownesses are much more important than compressional-wave slownesses in the amplification of earthquake ground motion.

Procedures for Comparing Models

Central to our article are the ways in which we compare the models from the various interpretations. Traditionally, the comparisons are done visually by plotting the velocity versus depth for various models. As we discussed earlier, we prefer plots of slowness versus depth in such comparisons, as they better illustrate differences for high values of slowness rather than for low values of slowness. High values of slowness are generally found near the surface and are more important in determining site amplification for engineering purposes than are the generally lower values of slowness at greater depths.

Another basis for comparison are average slownesses from the surface to various depths. A commonly used depth is 30 m; this average is used in classifying sites in some modern building codes (Dobry *et al.*, 2000; Building Seismic Safety Council (BSSC), 2004) and is used to characterize site response in recent ground-motion prediction equations (e.g., Power *et al.*, 2008). Average velocities for a number of the models discussed here were tabulated by Stephenson, Louie, *et al.* (2005) for depths of 30, 50, and 100 m and by Asten and Boore (2005b) for depths of 30, 85, 185, and 293 m. In this article, we tabulate the average slownesses for depths of 5, 10, 20, 30, 40, 80, and 160 m.

Plots of slowness and tabulated values of average slowness do not provide quantitative estimates of the consequences of different models for one of the most important practical engineering uses of slowness models: the amplification of ground motion due to the near-surface

Table 2
List of Measurements and Interpretations for which Results Are Presented in This Article

Method	Selected Reference (in Asten and Boore, 2005a, if possible)
Invasive Methods	
Suspension PS velocity logger (SPSVL)	http://www.geovision.com/PDF/M_PS_Logging.PDF, last accessed May 2008
Surface source-downhole receiver: using borehole (SSDHR-BH)	Boore and Thompson (2007)
Surface source-downhole receiver: using SCPT (SSDHR-SCPT)	T. L. Holzer *et al.* (unpublished manuscript, 2008)
Noninvasive: Active Sources	
High-resolution reflection/refraction (HRRR)	Williams *et al.* (2005)
Spectral analysis of surface waves (SASW)	Bay *et al.* (2005)
Multichannel analysis of surface waves (MASW)	Stephenson, Williams, *et al.* (2005)
Noninvasive: Passive Sources	
2D receiver array	
Spatial autocorrelation (SPAC)	Hartzell *et al.* (2005)
Multimode spatial autocorrelation (MMSPAC)	Asten (2005)
1D receiver array	
Refraction microtremor (ReMi)	Stephenson, Williams, *et al.* (2005)
0D receiver array	
Horizontal/Vertical Spectral Ratios (HVSR)	D. H. Lang (personal comm., 2004) and Lang and Schwarz (2005)
Noninvasive: Combined Active and Passive Sources	
MASW + frequency-wavenumber array analysis (MASW + FK)	Yoon and Rix (2005)
MASW + microtremor array method (MASW + MAM)	Hayashi (2005)

The abbreviations are used in the figures showing the results.

sediments. For this reason, we prefer comparisons of the amplifications of the models rather than the slowness models themselves. We present the results of three methods of estimating linear amplification: empirically based amplifications using the average slowness to 30 m, simplified amplifications based on the square root of the effective seismic impedance (SRZ), and calculations of linear site response for plane *SH* waves that account for all reverberations within the layers. We discuss the amplification calculations in more detail in the section on results from CCOC/WSP.

While we are primarily interested in slowness values averaged over depth intervals, as these are of most importance to site amplification, we recognize that point estimates of slowness are useful in engineering applications as well, such as in studies of liquefaction potential.

Results: CCOC/WSP

Location

The locations of the borehole at the CCOC and WSP are shown in Figure 4. Unlike CCOC, the access at WSP is unrestricted and there is more room in which to conduct measurements. For these reasons, most measurements were made at WSP. Note that the two sites are separated by about 200 m and are both located along the course of a nearby stream (Coyote Creek) that is incised about 10 m below the surrounding ground level. According to Wentworth and Tinsley's (2005) analysis of the history of sediment deposits as inferred from analysis of cuttings, cores, and logs from the CCOC borehole, little lateral variation is expected in the slownesses of the materials beneath both sites.

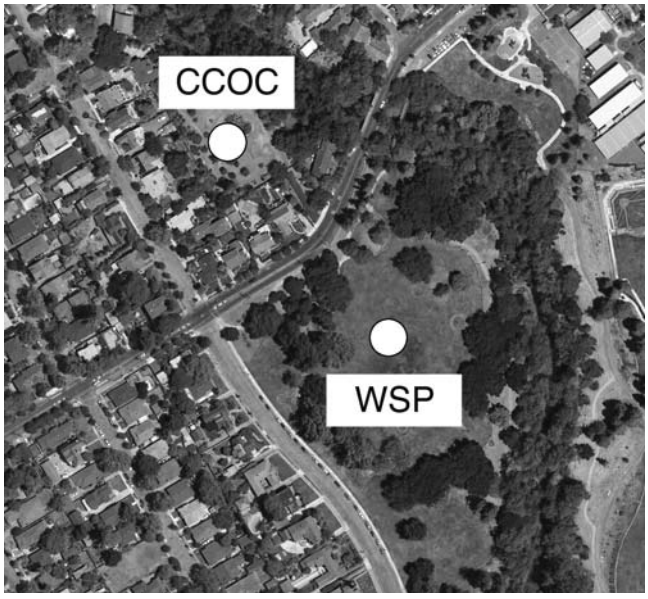

Figure 4. Detailed location map of the CCOC and WSP blind interpretation exercise. The coordinates of CCOC are −121.86835° E, 37.33702° N (NAD27 datum), and CCOC and WSP are separated by about 200 m. The line of trees follows the course of Coyote Creek. (The aerial image came from Google Earth, http://earth.google.com, last accessed May 2008.)

Sources of Models

All of the models were sent to us in the form of American Standard Code for Information Interchange (ASCII) files and spreadsheet files by the investigators. Most of the models for CCOC/WSP are included in individual papers and presentations gathered together by Asten and Boore (2005a). The specific models are listed in Table 3. When reports contained multiple interpretations, we chose the single interpretation preferred by the investigators. We include this information in Table 4. For models interpreted by Lang from horizontal/vertical spectral ratio (HVSR) measurements and by Stephenson from refraction microtremor (ReMi) measurements, we used results subsequent to those submitted for the May 2004 workshop. (See Table 2 for the definition of abbreviations such as HVSR and ReMi used to describe the measurements.) While these results are not strictly blind, we are convinced that the revised models did not make use of the information learned at the workshop. Lang's initial measurements were clearly in error, and he based his revised model on new measurements; Stephenson chose to derive his preferred model as the geometric mean of models from extremal estimates of the dispersion curves rather than from a single preferred dispersion curve.

Reference Model

In our comparisons of both the slownesses and the amplifications, we find it desirable to define a reference model that we hope is close to the actual slowness under the site. It is tempting to use the SPSVL as the reference model, as being based on invasive measurements, it is a direct measure of wave slowness. In addition, in comparison to the other invasive models, it has better vertical resolution (the dominant frequency of the waves used to measure travel time is near 1000 Hz, as opposed to the approximately 50-Hz waves used by the other invasive methods) and extends to greater depth. Some might object to the large, random-appearing variation of the slowness with depth (Fig. 5). These variations, however, coincide very closely with the grain sizes of the sediments (also shown in Fig. 5), with low and high velocities corresponding to the cycles of fine- and coarse-grained materials, respectively. This correlation between the SPSVL model and the material variations led Wentworth and Tinsley (2005) to conclude that the variations in the SPSVL models are real and are not due to interpretation error.

But in spite of the results presented in Figure 5, we do not use just the SPSVL model as the reference model; instead, we use an average of the slownesses from all three invasive methods. We elaborate on this decision here. The first invasive measurements were from a seismic cone penetration test (SCPT) to a depth of 37 m, performed by Noce at the site of the borehole before the hole was drilled (Noce and Holzer,

Table 3

Specific Models and Average Shear-Wave Slowness (S_S) to Indicated Depth for All Interpretations and All Sites

Method and Reference	d_{max}	$\bar{S}_S(30)$	$\bar{V}_S(30)$	$\bar{S}_S(5)$	$\bar{S}_S(10)$	$\bar{S}_S(20)$	$\bar{S}_S(40)$	$\bar{S}_S(80)$	$\bar{S}_S(160)$
CCOC (CCOC)									
Reference Model (see text)	293	4.42	227	4.74	4.76	4.76	4.19	3.45	2.71
SSDHR-BH (Gibbs, WC [2003]; Boore, 2003a)	184.5	4.29	233	4.56	4.56	4.56	4.11	3.4	2.68
SSDHR-SCPT (Holzer, WC [2004])	37.2	4.23	237	4.78	4.78	4.66			
SASW (Bay *et al.*, 2005)	24.7	4.82	208	5.65	5.37	5.09			
SASW (Stokoe, WC [2004])	34	4.81	208	5.81	5.47	5.2			
CCOC (WSP)									
SSDHR (Holzer, WC [2005])	21	4.44	225	4.44	4.44	4.44			
HRRR (Williams *et al.*, 2005)	85	4.55	220	4.98	4.66	5.02	4.09	3.36	
SASW (Bay *et al.*, 2005)	27.1	4.87	205	6.5	5.83	5.18			
SASW (Kayen, 2005)	32.3	5.09	197	7.98	6.64	5.74			
SASW (Stokoe, WC [2004])	38	4.6	217	6.54	5.84	5.37			
MASW (Stephenson, Williams, *et al.*, 2005)	100	4.54	220	5.3	5.27	4.95	4.1	2.97	
MMSPAC (Asten, 2005)	3420	4.28	234	5.56	5.56	4.95	3.95	3.36	2.64
SPAC (Hartzell *et al.*, 2005)	350	4.11	243	5.85	5.85	4.85	3.72	3.1	2.47
ReMi (Louie, via Stephenson, WC [2005])	100	4.2	238	5.57	5.24	5.02	3.76	2.88	
ReMi (Stephenson, Williams, *et al.*, 2005)	100	4.35	230	4.9	4.88	4.65	4.05	3.12	
HVSR (Lang, WC [2004])	521	3.57	280	5.33	4.33	3.79	3.35	2.84	2.42
MASW + MAM (Hayashi, 2005)	178.1	4.78	209	7.31	6.51	5.42	4.34	3.48	3.02
MASW + FK (Yoon and Rix, 2005)	130	4.49	223	6.35	6.11	5.01	4.09	3.2	
GUAD									
MASW (Stephenson, WC [2005])	60	4.29	233	6.76	5.77	4.92	3.96		
SASW (Stokoe, WC [2004])	22.6	4.14	242	6.15	5.43	4.71			
MMSPAC (Asten, WC [2006])	4875	4.49	223	5.26	5.26	4.68	4.12	3.45	2.81
ReMi (Louie, via Stephenson, WC [2005])	210.5	3.66	273	6.29	4.97	4.17	3.37	2.95	2.45
ReMi (Stephenson, WC [2005])	180	3.04	329	3.31	3.31	3.34	2.88	2.88	2.48
HVSR (Lang, WC [2005])	520	4.55	220	4.55	4.55	4.55	3.98	3.12	2.62
MGCY									
Reference Model (SPSVL data, 5m average)	260	2.28	439	3.56	2.95	2.55	2.06	1.71	1.48
HRRR (Stephenson, WC [2005])	30	2.24	447	3.76	2.93	2.45			
MASW (Stephenson, WC [2005])	70	2.51	398	3.38	3.04	2.73	2.28		
MMSPAC (Asten, WC [2006])	4940	2.45	409	3.17	3.17	2.63	2.29	1.93	1.52
ReMi (Louie, via Stephenson, WC [2005])	100	2.42	413	4.41	3.27	2.7	2.23	1.94	
ReMi (Stephenson, WC [2005])	160	2.46	406	2.96	2.96	2.62	2.26	1.92	1.52
STGA									
Reference Model (SPSVL data, 5-m average)	260	2.45	408	4	3.55	2.67	2.46	2.08	1.67
HRRR (Stephenson, WC [2005])	30	2.11	475	3.76	3.23	2.44			
MASW (Stephenson, WC [2005])	80	2.66	376	3.31	3.66	2.88	2.58	2.16	
MMSPAC (Asten, WC [2006])	5185	2.6	385	3.03	3.03	2.77	2.52	2.23	1.82
ReMi (Louie, via Stephenson, WC [2005])	189.2	2.45	409	2.9	2.63	2.49	2.35	2.09	1.56
ReMi (Stephenson, WC [2005])	190	2.47	404	2.75	2.75	2.82	2.33	2.12	1.63
STPK									
Reference Model (SPSVL data, 5-m average)	300.2	3.46	289	5.2	4.72	3.89	3.11	2.45	1.89
MMSPAC (Asten, WC [2006])	5026	3.68	272	4.17	3.94	4.14	3.36	2.79	2.12
HVSR (Lang, WC [2005])	630	2.5	400	2.5	2.5	2.5	2.41	2.27	2.16

(*continued*)

Table 3 (*Continued*)

Method and Reference	d_{max}	$\bar{S}_S(30)$	$\bar{V}_S(30)$	$\bar{S}_S(5)$	$\bar{S}_S(10)$	$\bar{S}_S(20)$	$\bar{S}_S(40)$	$\bar{S}_S(80)$	$\bar{S}_S(160)$
WLLO									
Reference Model (average S_s SSDHR models)	99	3.98	252	6.34	5.54	4.8	3.68	2.85	
SSDHR-BH (D. M. B. analysis, Gibbs data)	99.5	3.97	252	6.62	5.7	4.79	3.68	2.85	
SSDHR-SCPT (D. M. B. analysis, Holzer data)	23.5	4.26	235	6.05	5.37	4.8			
MMSPAC (Asten, model WLLO3a, WC [2006])	1220	4.1	244	6.06	5.41	4.63	3.83	3.05	2.28

Note that no average slowness is shown for depths exceeding the maximum depth of a model (d_{max}, in meters). Also shown are the average shear-wave slowness and velocity to 30 m ($\bar{S}_S(30)$ and $\bar{V}_S(30)$), with the lowest-most layer extrapolated to 30 m if needed. Written communication to the first author is denoted by WC. Note that most of the models attributed to Stephenson, WC (2005) are discussed in Stephenson, Louie, *et al.* (2005). No average slownesses are given for the SPSVL model because it does not extend to the surface; assumptions were made by the first author in extending the model to the surface when constructing the reference model for each site. The units of slowness and velocity are sec/km and m/sec, respectively.

2003). Next came the SPSVL measurements, made by Steller in the uncased borehole to a depth of 293 m, and finally came the measurements made by Gibbs in the PVC-cased borehole to a depth of 184 m, with a surface source and a downhole receiver, using procedures described by Boore (2003a) and by Boore and Thompson (2007). In the measurements made by Noce and by Gibbs, a surface source and a downhole receiver were used, so we use the abbreviation SSDHR for the methods, appending SCPT and BH for the two surveys, respectively (where BH stands for borehole). As shown in figure 7 of Boore (2006), the travel times from the surface to depth for the two SSDHR surveys are very similar. The travel times are consistent with a pronounced layer of coarse material from 19 to 23 m in depth having low values of slowness compared to the surrounding material. This layer shows up clearly on the SCPT friction ratio and tip resistance measurements (see fig. 4 in Wentworth and Tinsley, 2005), and age measurements from cores show the low slowness layer to be the base of the Holocene deposition cycle, deposited unconformably on Pleistocene deposits (Wentworth and Tinsley, 2005). We discuss this in some detail because there is a distinct mismatch in the SSHDR models and the SPSVL model at depths less than about 30 m, with the SPSVL model having higher values of slowness on average. As we will

Table 4

Models Used When Multiple Models for a Given Investigator Team Were Available

Site	Investigator(s)	Model Used
CCOC	Bay *et al.*	Model from forward modeling
CCOC	Stokoe	Average of upper and lower bound models for CL2 profile (closest to borehole)
WSP	Asten	pkdec2
WSP	Bay *et al.*	Model from forward modeling
WSP	Hartzell	Model using SPAC analysis
WSP	Lang	Model provided in October 2004
WSP	Stephenson	Model provided in March 2005
WSP	Stokoe	Average of upper and lower bound models
WLLO	Asten	WLLO3a

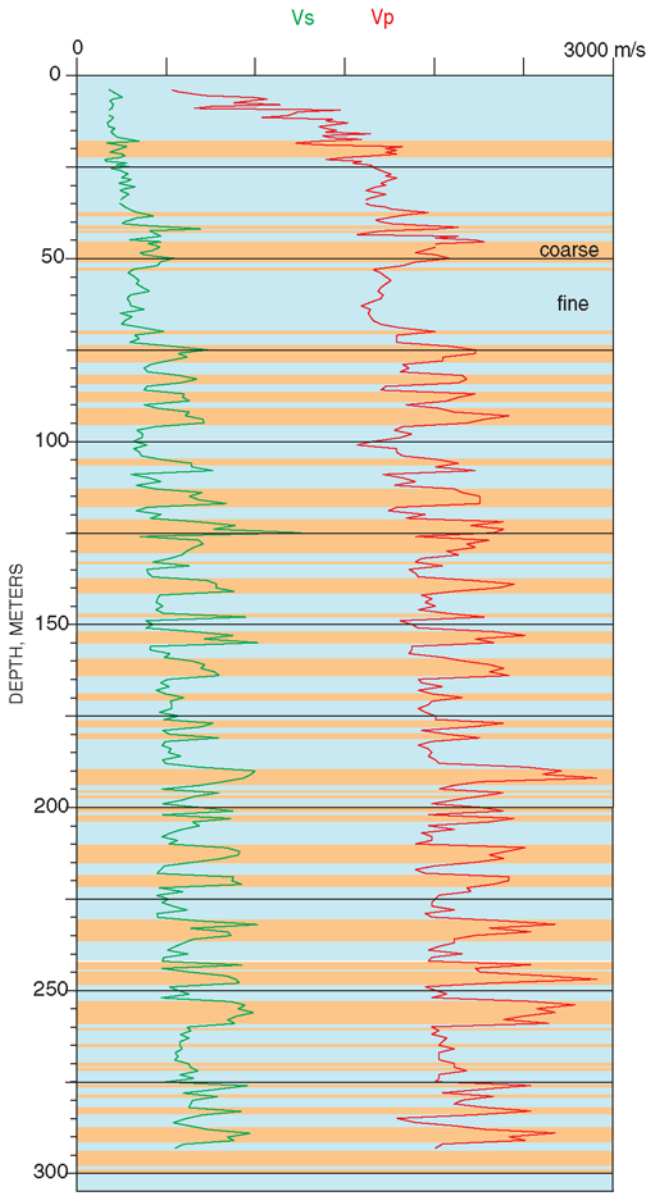

Figure 5. Correlation of SPSVL velocities for *P* and *S* waves with fine-grained layers (blue) and coarse-grained layers (orange). The grain sizes were taken from the drill logs; modified from Wentworth and Tinsley, 2005.

show later, the slownesses from the noninvasive measurements are also, on average, higher than those obtained from the SSDHR measurements. This, in combination with our experience comparing SSDHR-BH and SPSVL models at a number of sites, would suggest that we should use the SPSVL model as the reference model. But because of the differences seen at CCOC for depths less than about 30 m, we decided to form a reference model by averaging the slownesses from each intrusive model at each depth (of course, if a slowness value was not available because the depth exceeded the depth of the model, we used what was available). We used averages of the SPSVL model over 5-m depth intervals rather than the actual values of slowness in order to reduce the variability somewhat (full-reverberation amplifications using averaging intervals ranging from 0.5 to 10 m were almost identical for frequencies less than 10 Hz, which is consistent with an example shown in Boore and Thompson [2007] for a different site with similar variability to that in the SPSVL model). We also used reinterpretations by the first author of the SSDHR-BH and SSDHR-SCPT travel times, interpreted using the method of Boore and Thompson (2007), in an attempt to resolve finer variations than in the original models submitted for the blind interpretation exercise.

It is important to point out that differences of slowness from a specific model from the reference model do not necessarily imply an error in the specific model, for as G. Rix (personal comm., 2004) points out, "each type of seismic measurement is very different and captures a different aspect of the properties at the site. For example, the suspension PS logger (SPSVL), downhole test and surface wave test sample increasingly larger volumes of soil. If the soil conditions are heterogeneous (which they most certainly are), each test will measure different values of velocity" (Asten and Boore, 2005b). For many purposes, simply comparing one noninvasive model to another may be as meaningful as comparing a particular noninvasive model to the reference model—the variability gives an idea of the uncertainty of the estimates, even if we do not know the true model, particularly for models using the same type of measurement.

Slowness Comparisons

In this section, we show comparisons of slowness for the various models. Conspicuously absent in these graphical comparisons (with one exception) are error bars or uncertainty for each layer S_S and thickness parameter for each model. We know of no meaningful way to obtain uncertainties in a completely objective sense. Of the noninvasive measurements at CCOC, only one (Yoon and Rix, 2005) presented formal parameter uncertainties, derived from inversion theory as applied to the observed and fitted Rayleigh-wave dispersion-curve data, where observed Rayleigh-wave phase-velocity data were ascribed a 5% uncertainty. Estimates of uncertainty based on inversion theory assume data errors to follow Gaussian error distributions, whereas phase-velocity measurements in practice appear to be subject to biases rather than random error distributions. A review of dispersion curves derived by different methods reported in Asten and Boore (2005a) indicates that bias is a general problem, especially at low frequencies where the signal-to-noise ratio is a limitation with active methods, and array size (hence resolution) becomes a limitation for passive methods at high frequencies. For these or other unstated reasons, the majority of authors referenced in this study have not attempted to provide uncertainty estimates for derived parameters. The only formal uncertainties we show are for the SSDHR-BH model in Figure 6. These are the uncertainties from fitting lines to the travel-time versus depth data, but they do not include the uncertainties that can arise from systematic errors in picking the arrival times.

Comparisons of slowness for the models at CCOC are shown in Figure 6, with the invasive models and the spectral analysis of surface wave (SASW) noninvasive models shown in the left and right graphs, respectively. The invasive models are those submitted to the blind estimation exercise, not the first author's reinterpretation. We connected the individual SPSVL values in the left graph with lines, our justification coming from Wentworth and Tinsley's (2005) conclusion that the variations in the SPSVL slownesses are real. Although the near-surface detail is hard to see because of the depth scale used in the figure, the systematically larger values of the SPSVL slowness at shallow depths are readily apparent. It is also noteworthy that the SSDHR-BH model is very close to the depth-interval-averaged SPSVL model at deeper depths. Both models show a similar low-to-high-to-low variation in slowness from about 45 to 75 m (this variation corresponds to a thick layer of fine-grained sediments sandwiched between coarser-grained deposits, as shown in Fig. 5). As can be seen from Figures 7, 8, and 9, none of the noninvasive models show these variations. The two SASW models are quite similar to one another, although they depart systematically from the reference model (but recall our comment regarding possible reasons that the models might be different even if correct).

The models obtained from measurements at WSP are shown in Figures 7, 8, and 9. In each figure, the same models are shown with two depth scales: deep on the left and shallow on the right. Figures 7, 8, and 9 show models derived for the active-, passive-, and combined-source measurements, respectively. The active-source models do not extend to depths as great as the other models, and the slownesses for all models are systematically higher than the reference slownesses at depths less than about 10 m. We speculate that this might be due in part to the fact that the lawn at WSP is well watered, unlike the somewhat-compacted soil near CCOC. Brown *et al.* (2002, fig. 8) found a similar difference in near-surface slownesses at the Sepulveda Veteran's Administration Hospital in southern California. On the other hand, Figure 6 shows that the SASW measurements near CCOC are also higher than our reference model. As mentioned earlier, this might suggest that our reference model is incorrect at shallow depths, but we think our reasoning for including the other invasive models in deriving the reference model is sound.

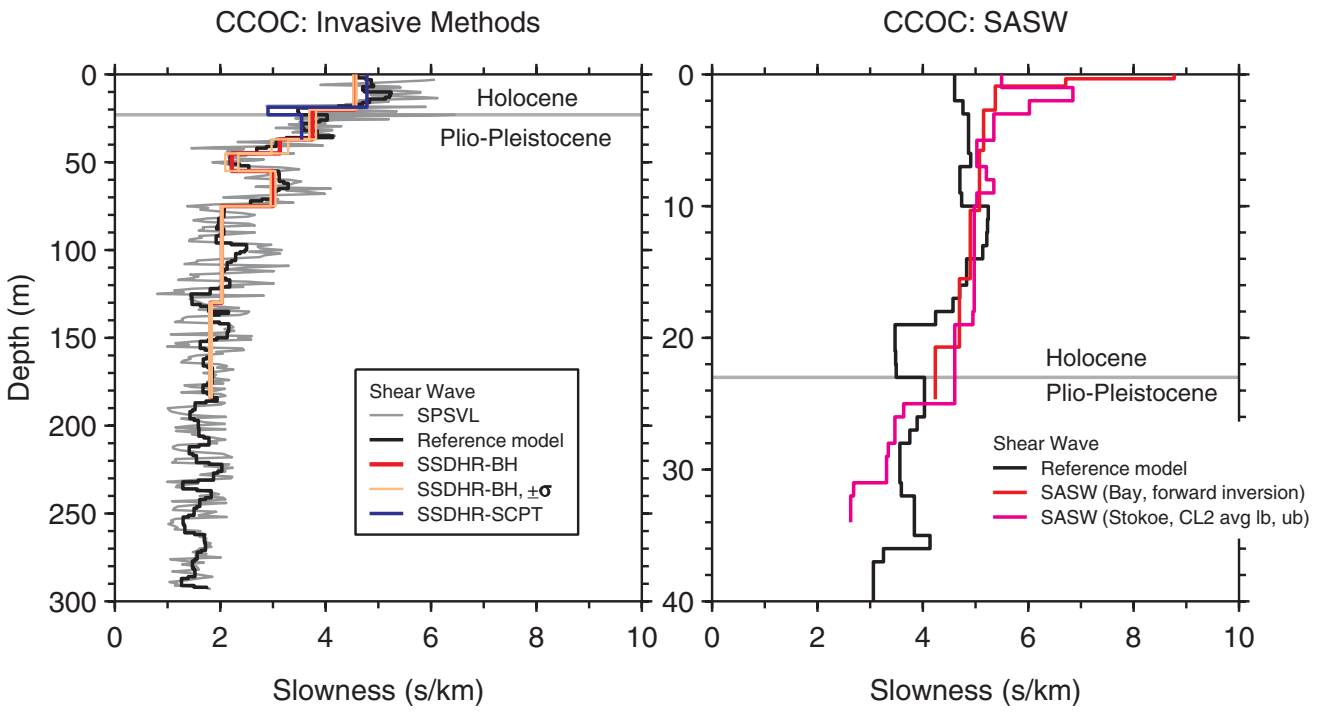

Figure 6. Slowness versus depth at CCOC from intrusive (left graph) and SASW (right graph) methods. The formal standard deviations of slowness for the SSDHR-BH model are indicated in the left graph. The depth scale for the right graph differs from the left graph because the SASW models extend only to about 34 m.

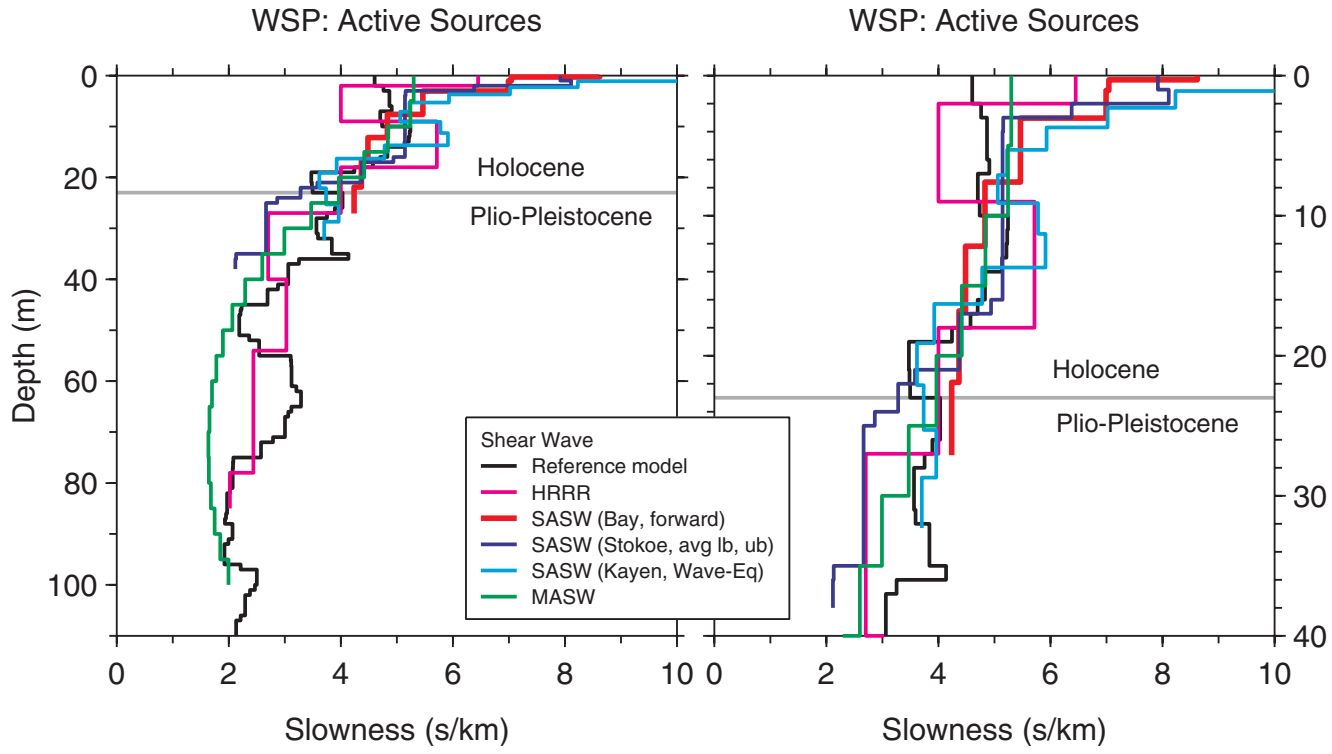

Figure 7. Slowness versus depth at WSP from active sources. The slowness for the Stokoe model is an average of their lower bound (denoted lb) and upper bound (denoted ub) models. The two graphs show the same models; only the depth scale has changed.

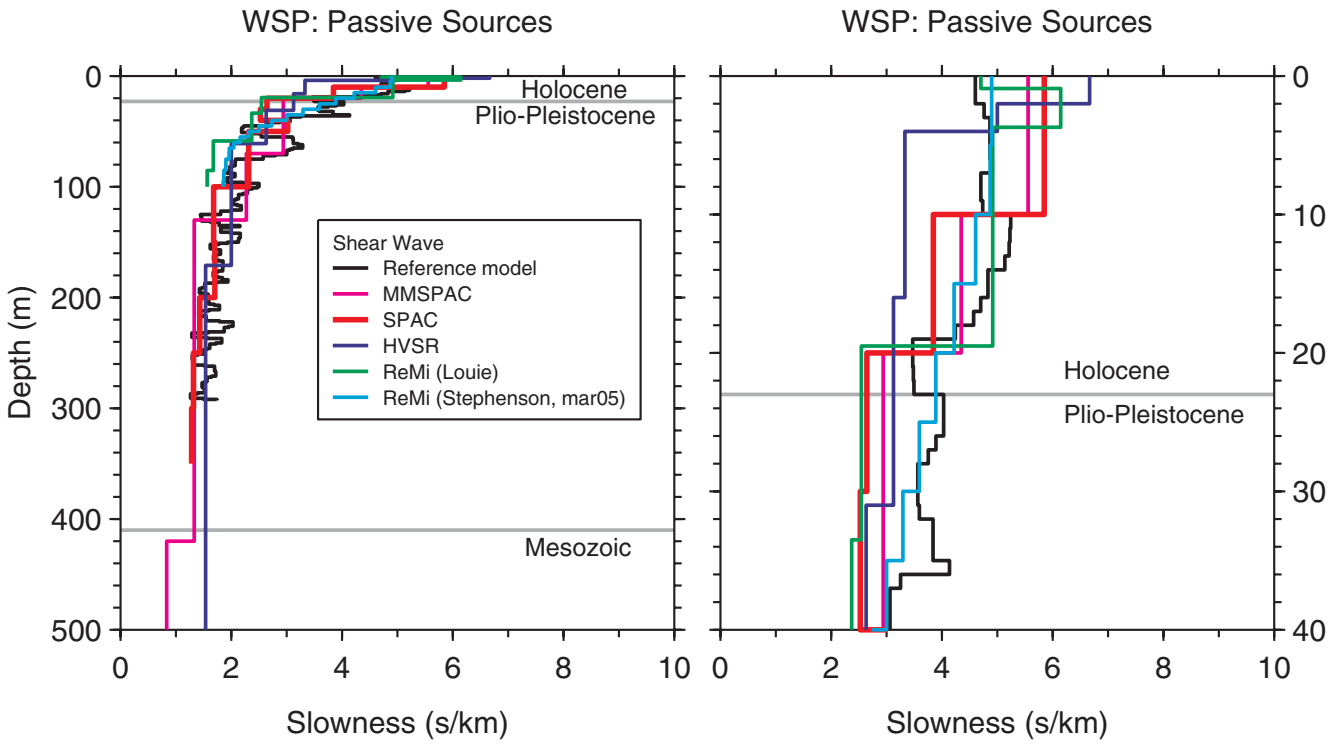

Figure 8. Slowness versus depth at WSP from passive sources. The two graphs show the same models; only the depth scale has changed.

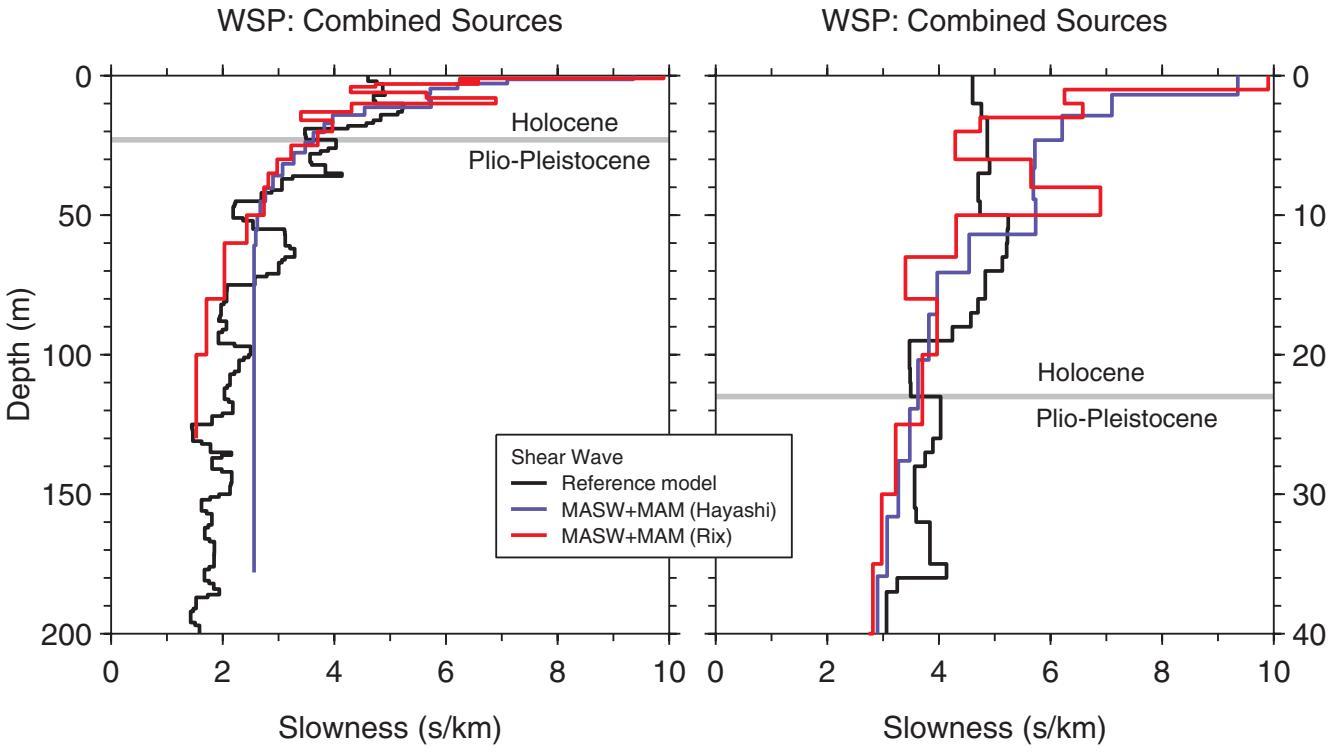

Figure 9. Slowness versus depth at WSP from interpretations using a combinations of active- and passive-source measurements. The two graphs show the same models; only the depth scale has changed.

Another way of comparing slowness that is directly related to several methods for approximating site amplification is to compute the average of the slowness from the surface to a depth. This is done using the equation

$$\bar{S}_S(z) = \frac{1}{z}\int_0^z S_S(\eta)\, d\eta. \qquad (1)$$

The result of doing that for the noninvasive and the reference model is shown in Figure 10. The average slownesses for a set of depths are tabulated in Table 3 for all sites. Note the convergence of the average slowness near 30 m (which is probably a coincidence) and the large scatter of average slowness at shallow depths. Note also that the models based on passive and combined active and passive measurements generally extend to greater depths than do those from active sources. The average slowness to 30 m is used to define site classes in the National Earthquake Hazards Reduction Program (NEHRP) building codes (Dobry *et al.*, 2000; BSSC, 2004); these classes are shown in Figure 10.

Amplification Comparisons

For all methods, we compute the amplification for each model and for a reference model. We then formed the ratio of the amplification from the specific model and from the reference model.

We first use the linear site amplification incorporated in the Boore and Atkinson (2008; hereafter, BA08) ground-motion prediction equations. The logarithm of the ratio of the amplification for a particular model with average slowness of $\bar{S}_S(30)$ and the amplification for the reference model with average slowness of $\bar{S}_S(30)_{\text{ref}}$ is given by

$$\ln A/A_{\text{ref}} = b_{\text{lin}} \ln[\bar{S}_S(30)_{\text{ref}}/\bar{S}_S(30)], \qquad (2)$$

where we have used equation (7) of BA08, written in terms of slowness rather than velocity. The coefficients b_{lin}, which are functions of the oscillator period, are given in table 3 of BA08 (these coefficients are based on the work of Choi and Stewart [2005]). We plot the results in Figure 11. The

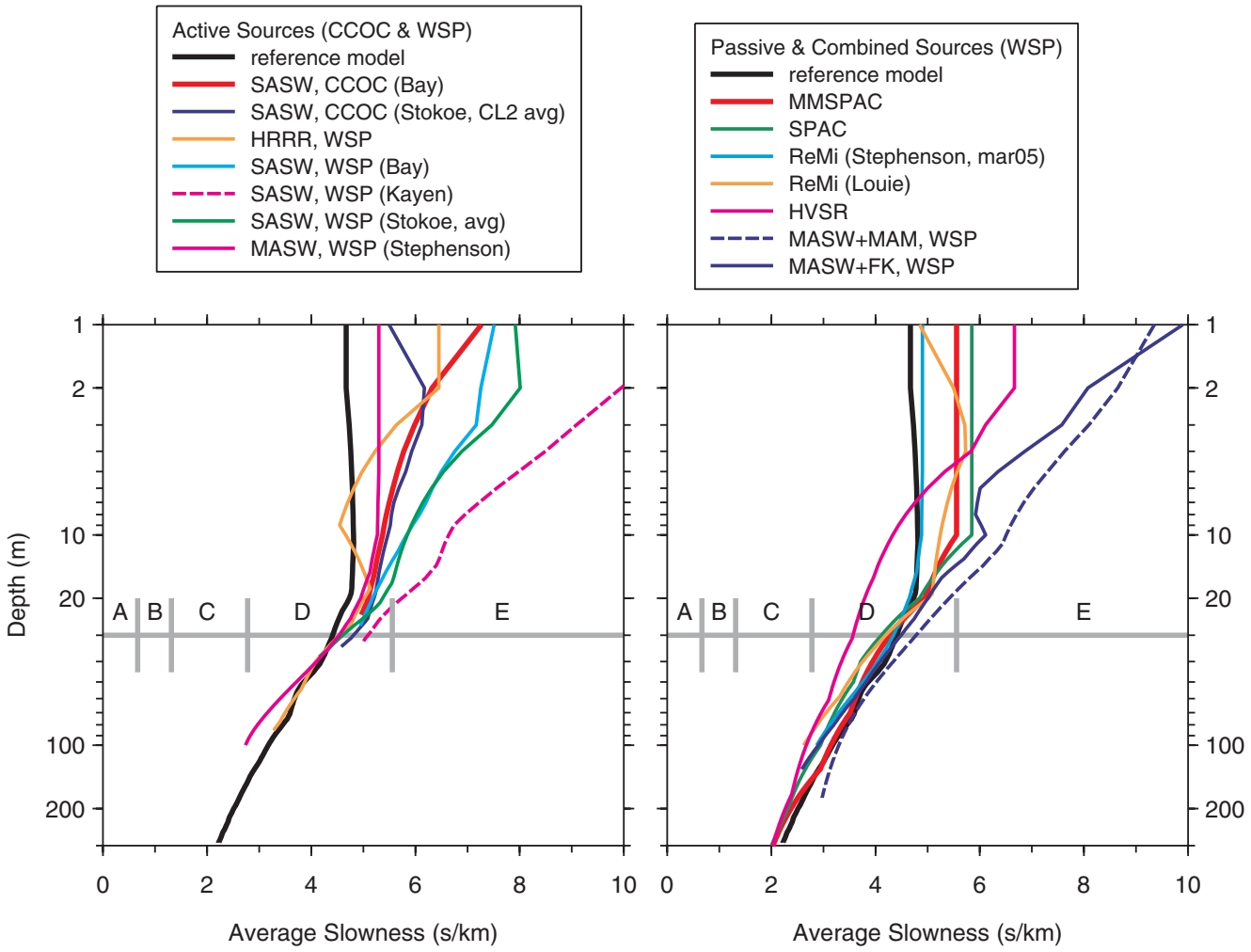

Figure 10. Average slowness from the surface to depth for noninvasive measurements (with the exception of the reference model, which is based on intrusive measurements). The NEHRP site classes C, D, and E, defined in terms of the average slowness to 30 m, are shown by the short vertical gray bars.

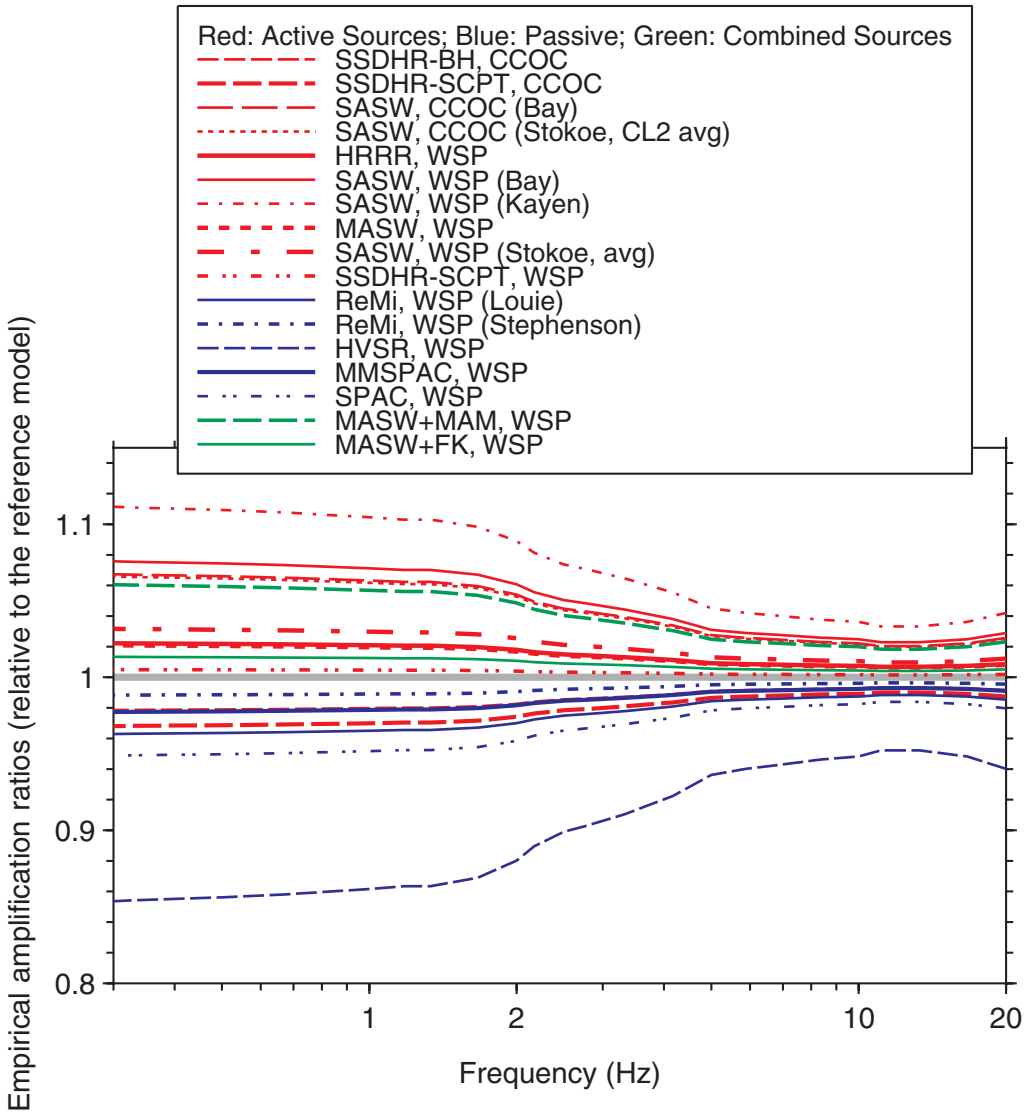

Figure 11. Amplifications at CCOC/WSP from the average slowness to 30 m from the various models, relative to the amplification for the reference model, using the linear amplification coefficients of Choi and Stewart (2005), as modified by Boore and Atkinson (2007, 2008).

ratios show that the predicted amplifications using $\bar{S}_S(30)$ from different methods differ by less than 10% for most cases. This is a trivial difference, so in this sense all of the methods and interpretations give comparable results in terms of a practical application. As a side note, it is interesting to observe that the models from interpretations of data collected using active sources give larger amplifications than do those from models using passive-source data, consistent with the larger values of $\bar{S}_S(30)$ for the active-source models seen in Figure 10. One reason for this might be that passive-source measurements are rarely designed to resolve near-surface properties, whereas active sources often use closely spaced sensors and high-frequency sources to obtain more accurate values of the near-surface properties. Because the slowness near the surface is generally larger than at depth, a more accurate model of these near-surface slownesses will lead to larger amplifications than from a model that averages the near-surface slowness with deeper slowness, resulting in a lower overall slowness for the near-surface layers and thus lower amplifications. A similar conclusion was reported by Cornou *et al.* (2007).

The similarity in the amplifications shown in Figure 11 is a result of the similarity of $\bar{S}_S(30)$ for the various models. As shown in Figure 10, the average slownesses have the fortuitous property that they tend to converge at 30 m. If the amplifications had been based on averages to shallower depths, we would expect to find larger variations in the amplification. To assess this, we computed amplifications based on the SRZ; see Boore (2003b) for a discussion of this method, which for any depth uses the average slowness to that depth as the inverse of the effective seismic impedance Z and assigns the resulting amplification to a frequency corresponding to a wavelength that is four times the depth. Other papers using ratios from SRZ amplifications in com-

paring slowness models include Boore and Brown (1998a,b), Brown *et al.* (2002), Stephenson, Louie, *et al.* (2005), and Cornou *et al.* (2007). The ratios of the amplification for a particular CCOC or WSP model and that for the reference model are shown in Figure 12 (note that the lowest frequency plotted for a given model corresponds to the quarter-wavelength equaling the deepest depth of a model). Clearly there is more variability than before, particularly at higher frequencies; this is expected from the slowness variations at shallow depths. But the variations are still relatively small, being largely less than 20%.

Although the SRZ amplifications are very useful for comparing the practical implications of various slowness models, they should be applied with caution when making amplification predictions for a given model. This is because the SRZ amplifications will always underestimate the fundamental model resonance of a system for which the slowness structure leads to a strong resonance. So why not base our comparisons on calculations of amplifications that account for all reverberations in the layered structure? There are two main reasons for this: (1) full-reverberation calculations require a model of slowness at depths generally deeper than the model under consideration (simply inserting a half-space beneath the model can lead to misleading results, unless a true impedance step exists at the base of the model) and (2) ratios of amplifications are sensitive to small differences in the frequencies of peaks and troughs in the individual amplifications, as we will illustrate shortly. For those reasons, we prefer to use ratios of SRZ amplifications as practically meaningful measures of differences between models.

To illustrate the full-reverberation calculations, we used the WSP SASW model of Bay *et al.* (2005) (for brevity, we refer to this in the following as the Bay model). We derived an extension of the reference model to greater depths by appending the SPSVL model at GUAD, averaged over 5-m intervals, from 291 to 410 m, and the generic rock model of Boore and Joyner (1997) with the depth scale adjusted so that the slowness at 410 m equals the estimated slowness of the Franciscan Complex (KJf) material (0.67 sec/km). The extended reference model and its components are shown in Figure 13. We then appended the extended reference model to the Bay model, starting at a depth corresponding to the bottom of the Bay model. As Figure 7 shows, the reference and the Bay slownesses are similar at the bottommost depth of the Bay model; therefore, the impedance contrast at the depth at which the two models were joined is small.

Having extended both the Bay and the reference models to a depth of 8 km, we then computed amplifications, relative to a half-space with a slowness of 0.286 sec/km (3.5 km/sec), assuming vertical incidence of plane *SH* waves and no damping in the layers. To account for damping, we applied the simple attenuation operator $\exp(-\pi\kappa f)$ to the amplifications, with $\kappa = 0.04$ sec. The amplifications for the two models (Bay and reference) computed for the two methods (SRZ and full reverberations) are shown in the left graph of Figure 14. As mentioned before, the SRZ

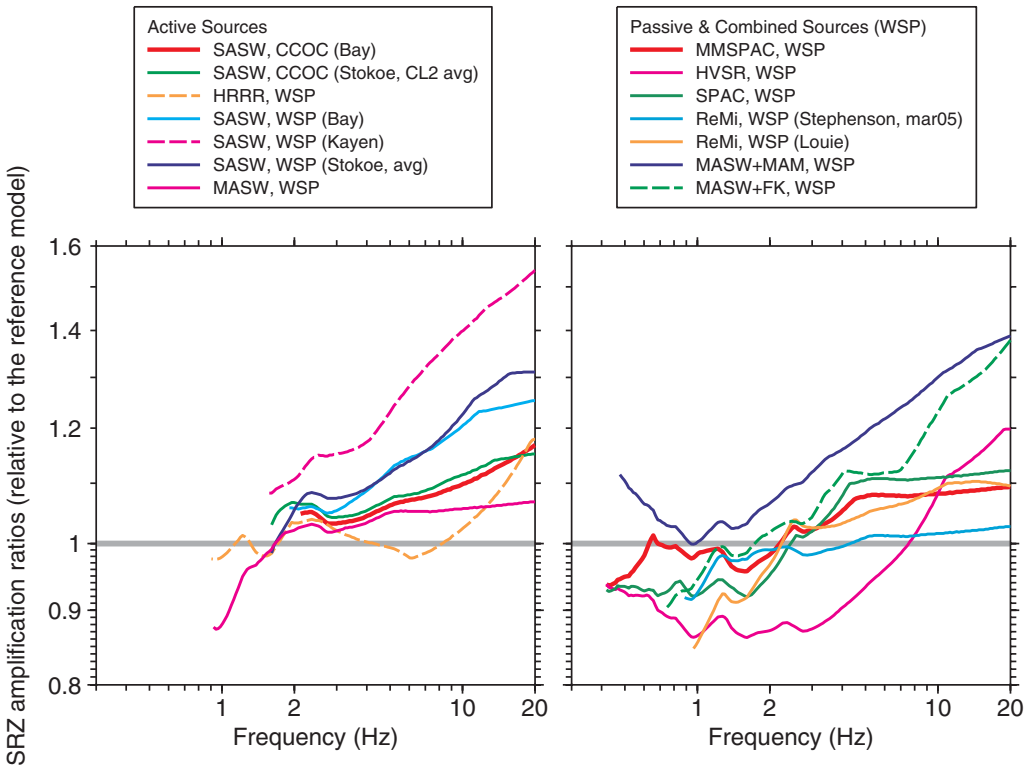

Figure 12. Amplifications at CCOC/WSP from the SRZ method (Boore, 2003b), relative to the amplification for the reference model.

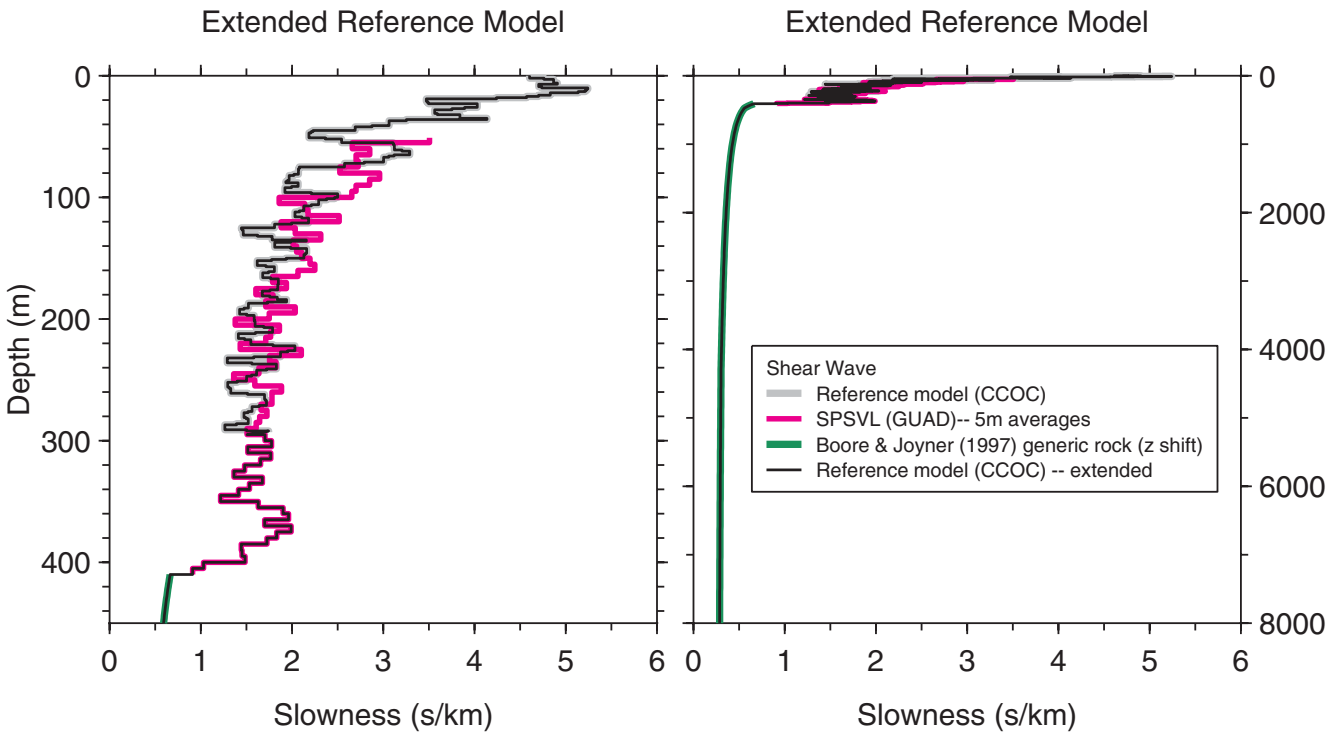

Figure 13. Slowness versus depth for the reference model extended to a depth of 8 km.

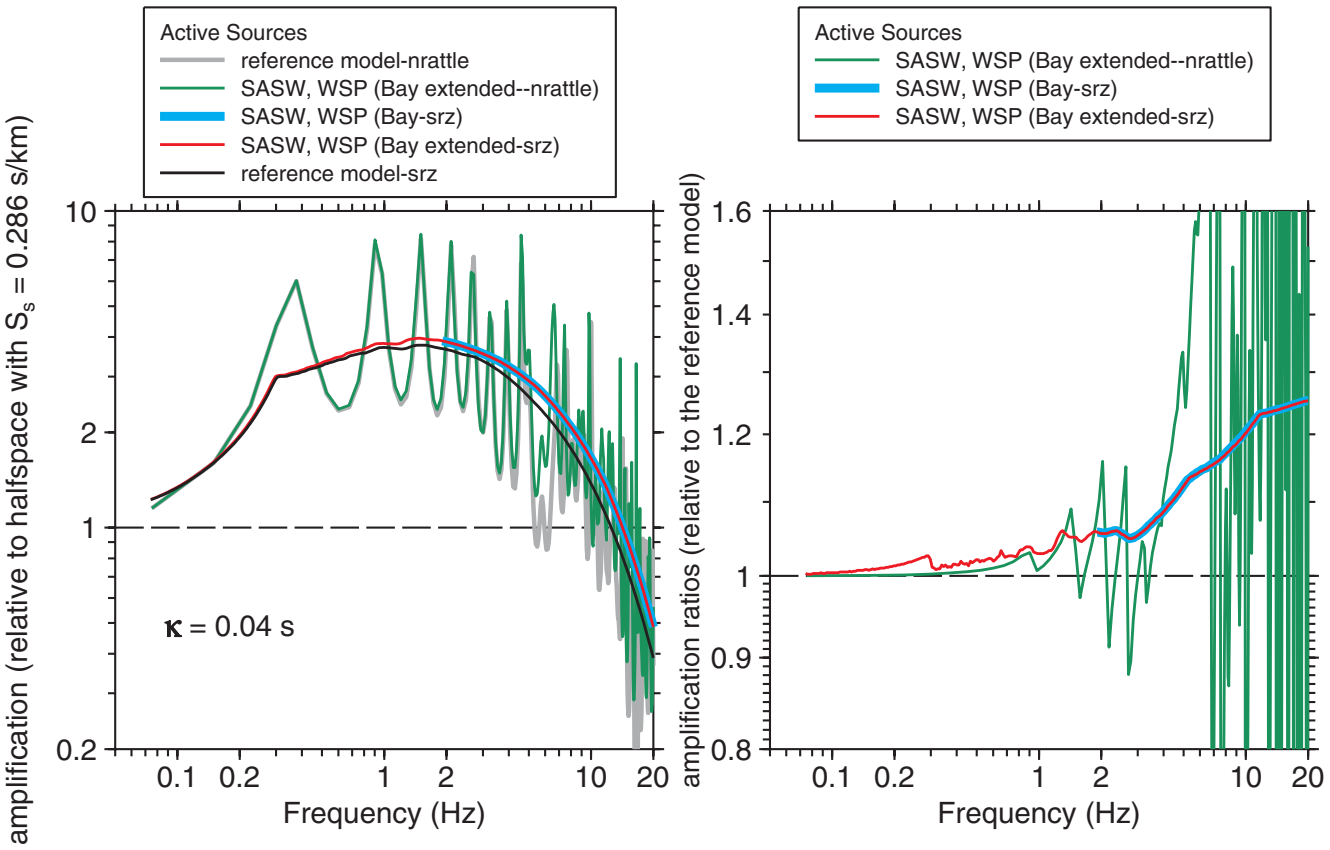

Figure 14. Left graph: amplifications relative to a 0.286 sec/km (3.5 km/sec) half-space using SRZ and full *SH*-plane-wave reverberation calculations for the reference model and for the WSP SASW model of Bay *et al.* (2005). Right graph: ratios of amplifications for the indicated models and the amplification for the reference model. See text for details.

amplifications seriously underestimate the fundamental resonance peak at about 0.3 Hz. For higher frequencies, the SRZ amplifications average the peaks and troughs of the full-reverberation amplifications, as expected (see Day, 1996). The ratios of the amplifications are shown in the right graph (the attenuation operator cancels out of the ratio). Also shown in the right graph are the ratios from the SRZ method without extension of the slowness models to greater depths; note that these ratios and those from the extended depth models are equal for frequencies greater than 1.9 Hz (the frequency corresponding to the bottom of the Bay *et al.* [2005] model), showing one of the advantages of the SRZ method: the amplifications for a depth-limited model do not depend on the unknown deeper structure for frequencies above the frequency associated with the maximum depth of the model. Also note that the ratio of the SRZ does a good job of capturing the mean ratio of the full-reverberation amplifications without the large peaks and troughs resulting from minor differences in the frequencies of the peak and troughs of the individual amplifications from the Bay and the reference models.

Results: GUAD, MGCY, STGA, STPK, and WLLO

Fewer slowness investigations were performed at the other sites, and for that reason our discussion of them is briefer than our discussion of the results for CCOC/WSP.

Slowness Comparisons

We limit our comparisons to graphs of slowness with depth. These are given in Figures 15–19. Note that no SPSVL slownesses are available for depths less than 50 m at GUAD because of the presence of steel casing in that depth range. In addition, no SSDHR investigations were made at GUAD, so we cannot construct a reference model at that site extending to the surface. No SSDHR measurements were made at MGCY, STGA, or STPK, so the reference model is derived solely from the SPSVL slownesses at those sites. Finally, no SPSVL measurements were made at WLLO, so the reference model was constructed by averaging the slownesses of the SSDHR-BH and SSDHR-SCPT models derived by the first author from travel times obtained by Gibbs and Noce; the reference model at WLLO only extends to 99 m.

While it is hard to generalize about the comparisons shown in Figures 15–19, the different methods give slownesses that are quite similar to one another. Particularly impressive is the agreement between the SPSVL slownesses and the deeper models from the HVSR and MMSPAC methods at GUAD and the MMSPAC method at STGA and STPK. We note that GUAD is the only site for which the borehole penetrated bedrock and for which SPSVL results are available; the bedrock depth is around 410 m, and the MMSPAC method identified a step decrease in slowness at 375 m. In addition, at WLLO, the MMSPAC method finds a step decrease in

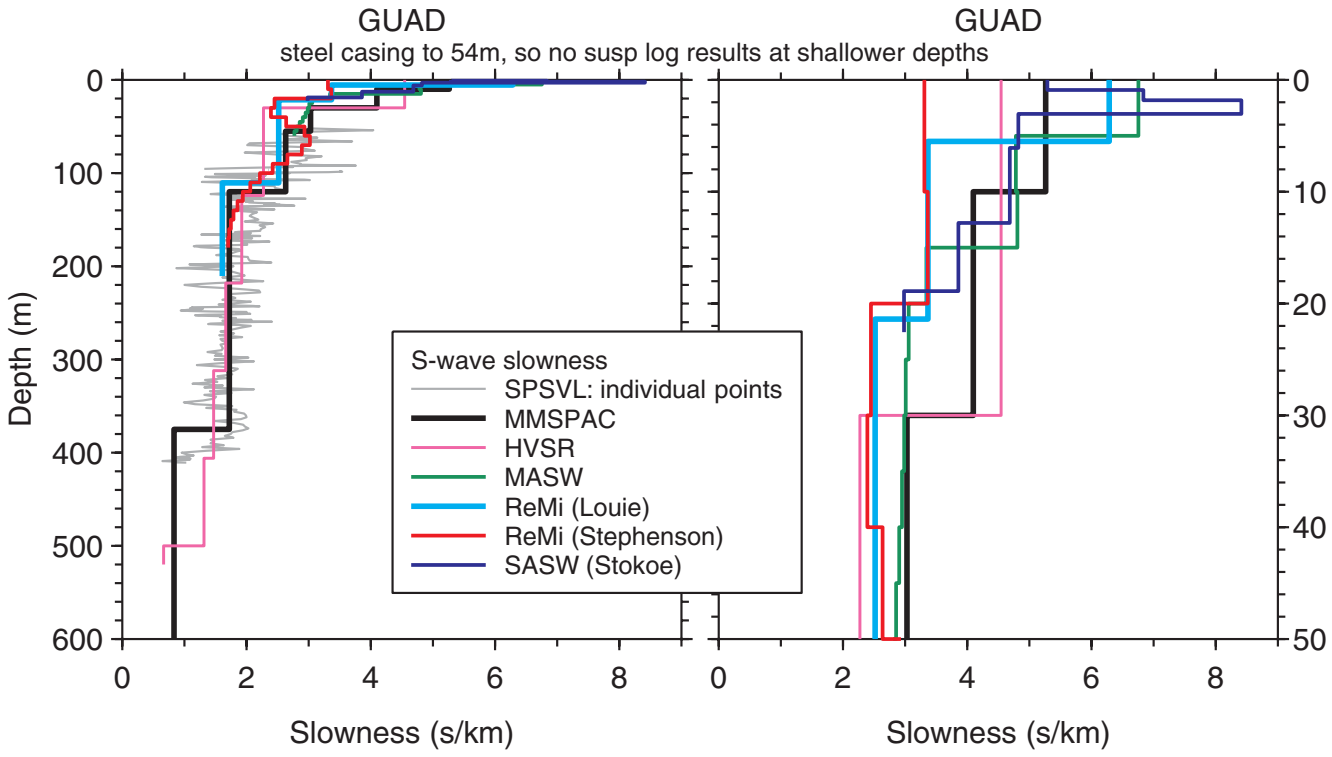

Figure 15. Slowness versus depth at GUAD. The two graphs show the same models; only the depth scale has changed.

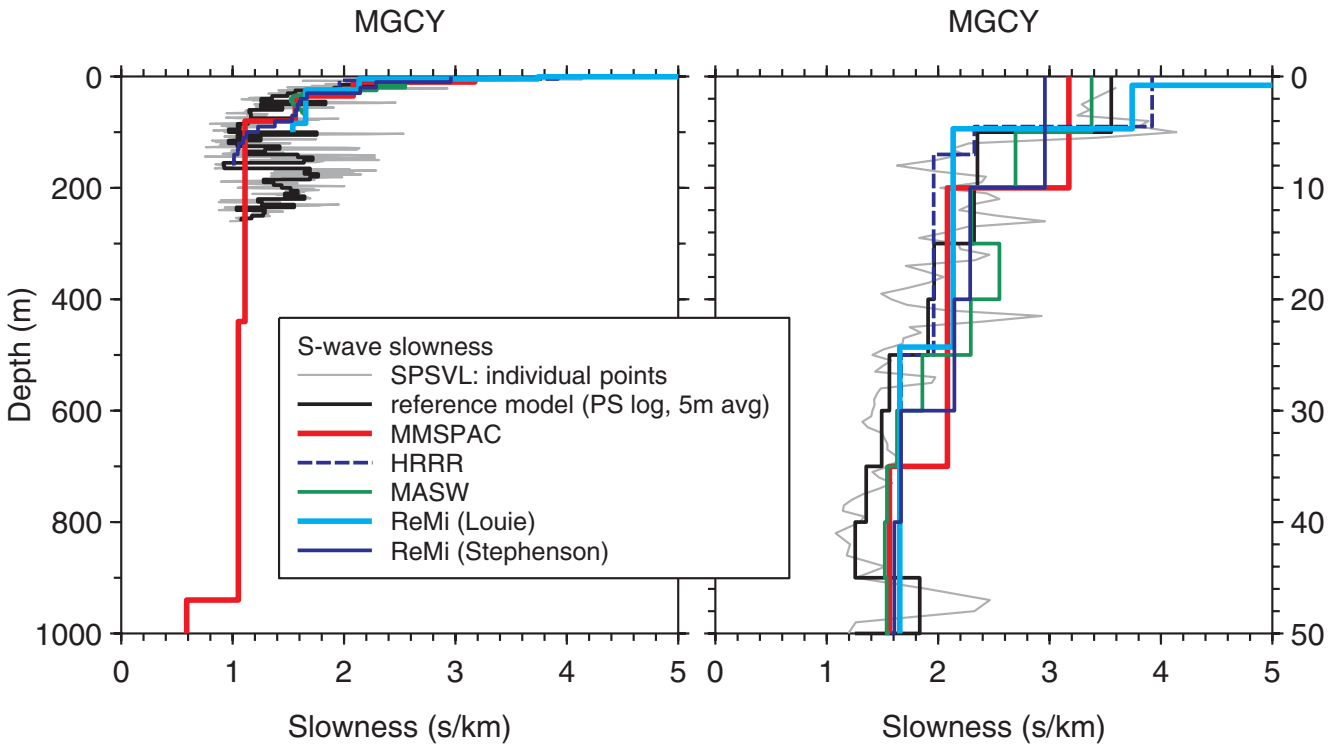

Figure 16. Slowness versus depth at MGCY. The two graphs show the same models; only the depth scale has changed.

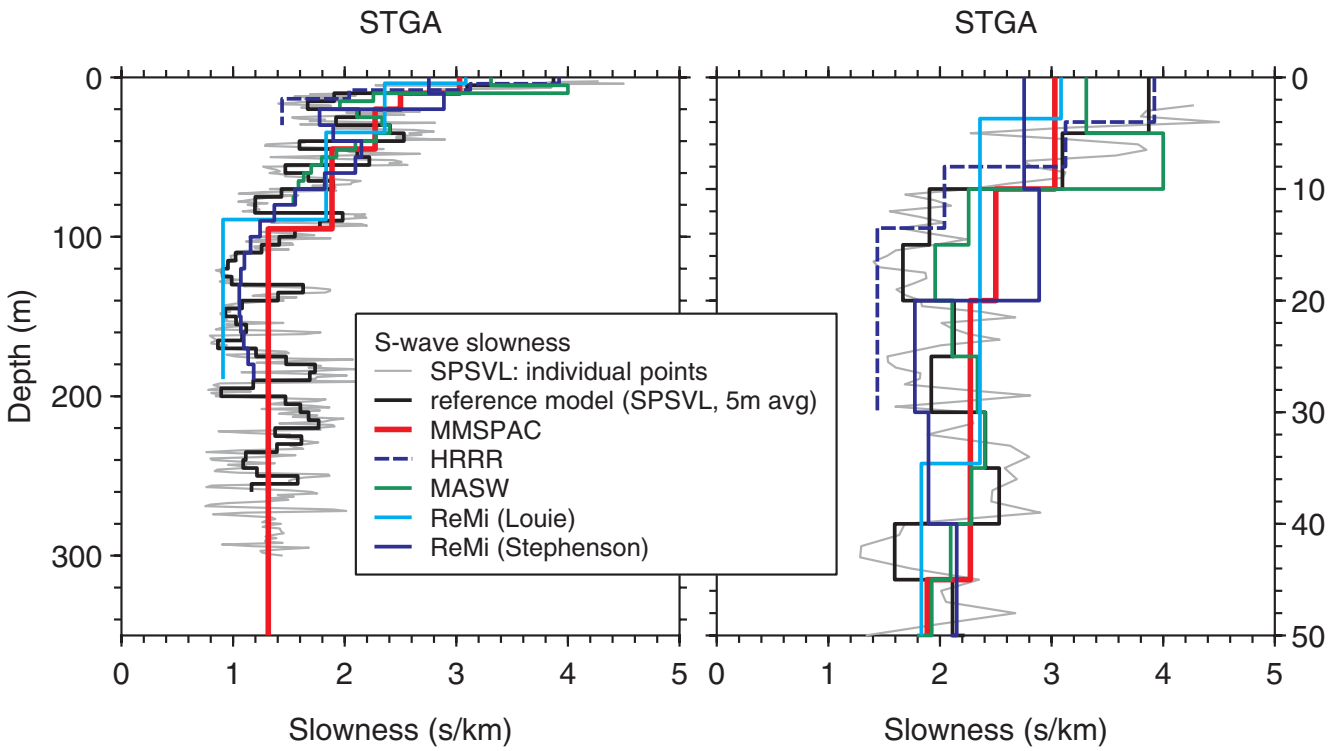

Figure 17. Slowness versus depth at STGA. The two graphs show the same models; only the depth scale has changed.

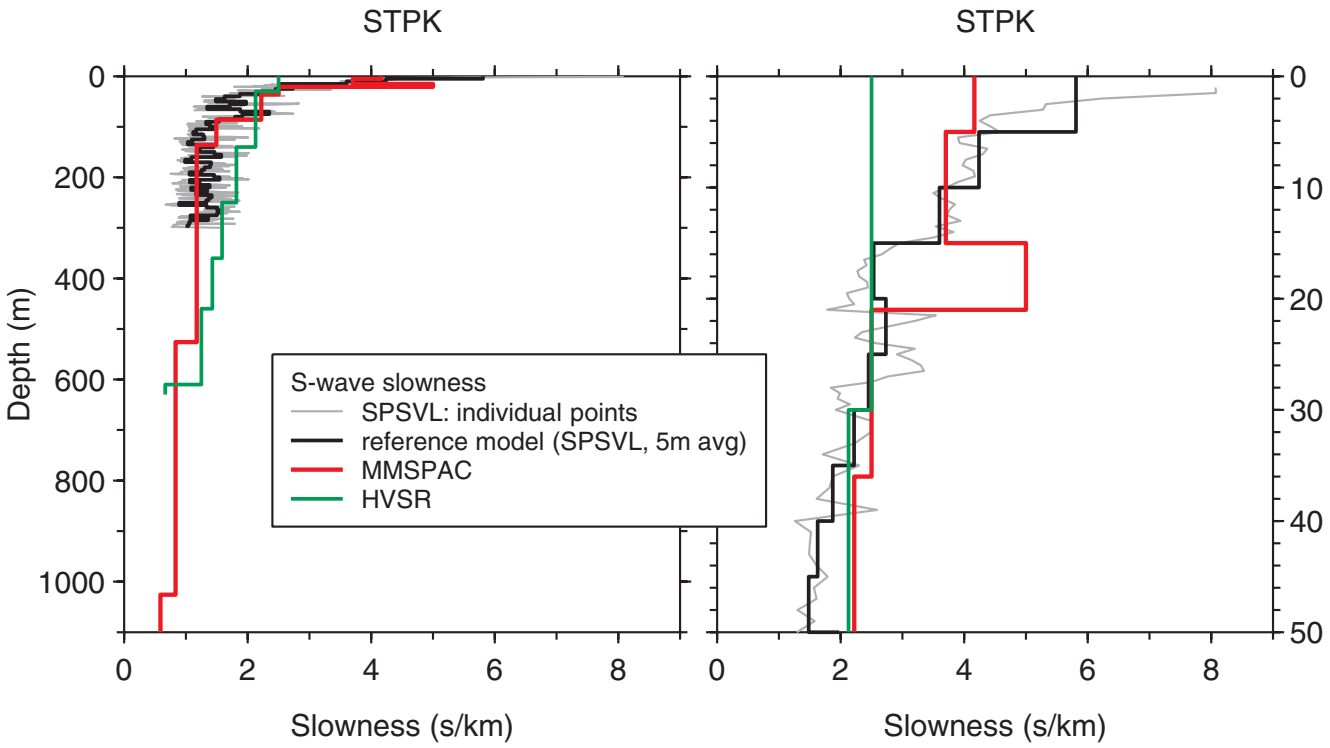

Figure 18. Slowness versus depth at STPK. The two graphs show the same models; only the depth scale has changed.

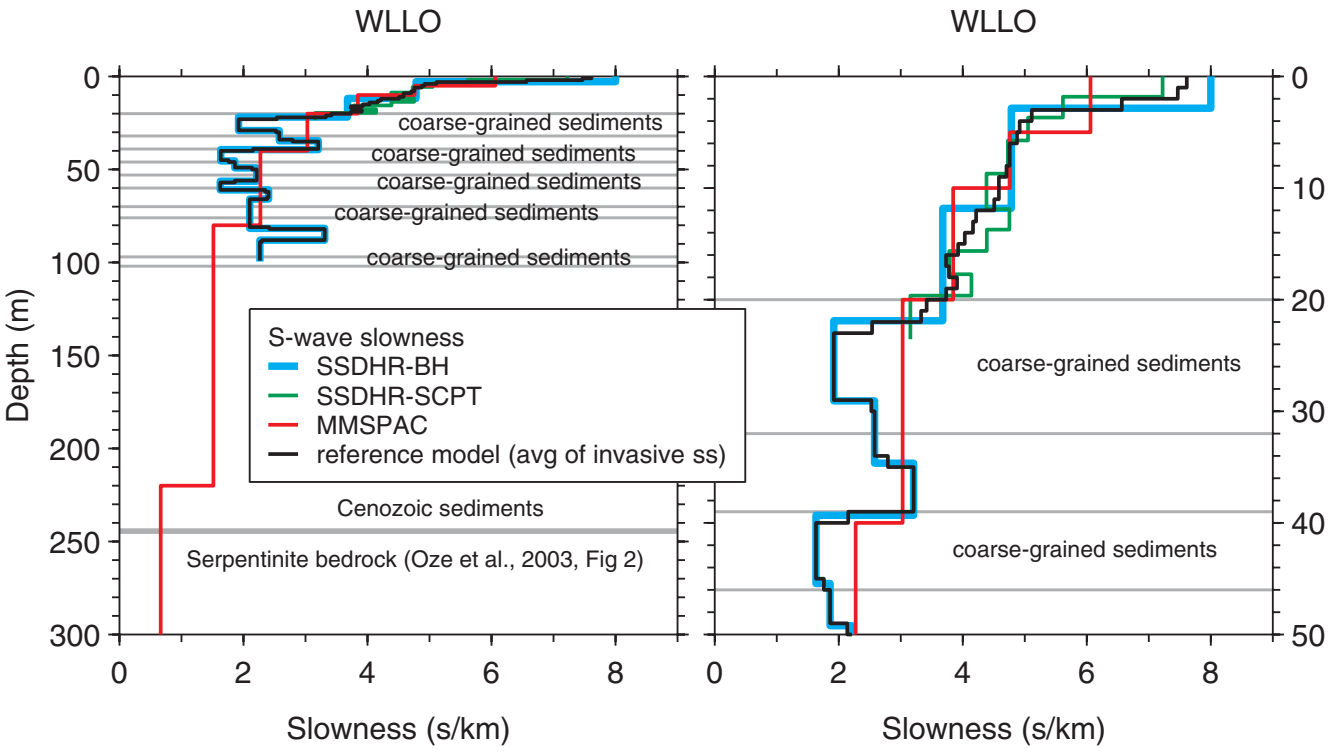

Figure 19. Slowness versus depth at WLLO. No SPSVL measurements were made at this site. The coarse- and fine-grained layering is indicated to show that generally the intrusive measurements agree with the slowness variation expected from the grain size: slower for coarse-grained material. Also indicated is the depth to the KJf bedrock, as determined from the drilling log (Oze *et al.*, 2003; Newhouse *et al.*, 2004). The two graphs show the same models; only the depth scale has changed.

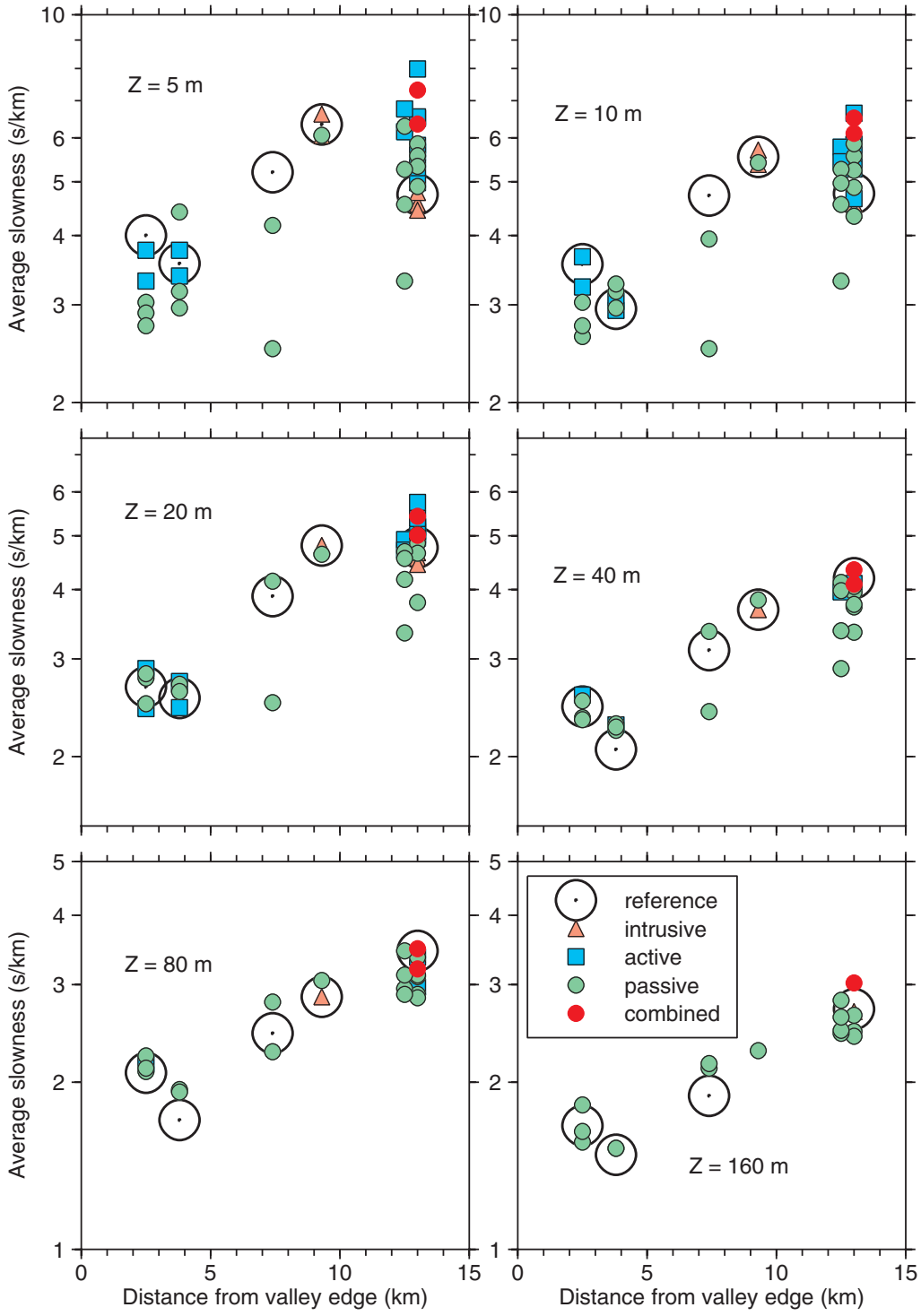

Figure 20. Average slowness to depths of 5, 10, 20, 40, 80, and 160 m (from Table 3), plotted against approximate distance from the edge of the Santa Clara Valley. The ordinate spans the same ratio of slowness for all graphs (a factor of 5). The different symbols indicate models grouped according to measurement method.

slowness at a depth close to that estimated for the bedrock depth (220 versus 241 m) (at WLLO, the borehole also penetrated bedrock, but no SPSVL measurements were obtained at that site).

Amplification Comparisons

We show no amplification ratios for the other sites, as the results are similar to those for CCOC/WSP in terms of overall variation (generally less than 10%). Stephenson, Louie, *et al.* (2005) include amplification ratio comparisons based on SRZ for several of the sites, although their reference models are not always the same as ours, leading to some differences in the details of the ratios (but with a similar overall finding regarding the variability of the amplification).

Slowness Variations across the Valley

Motivated by the systematic changes in slownesses for the SPSVL models in Figure 3, we show in Figure 20 the average slownesses for the different classes of models as a function of distance from the valley edge. Each graph corresponds to a different depth to which the slowness is averaged. We think that this figure is a useful summary of what we have found in this article. Taken as a whole, the average slownesses from all methods clearly show an increase with increasing distance from the valley edge. Of course, the large variations in slowness near the surface, obvious in Figure 3, exert a strong influence on the averages to deeper depths (in general, if the only variation in slowness is above a depth H_S, with a difference of average slowness to that depth for two sites given by ΔS_S, then the difference in slowness to a greater depth H_D will be given by $[H_S/H_D]\Delta S_S$). But Figure 3 shows that there are clear differences in slowness for depths as large as 300 m. We also see in Figure 20 that the variability between the models is greatest at shallow depths, and that the models using noninvasive active sources do not extend to depths as great as do those from passive sources.

Conclusions and Discussion

In general, the various methods yield slowness models similar enough to one another that site amplifications based on any one model are within about 10%–20% of those from other models. Models based on measurements using passive sources extend to greater depths than those from models based on active-source measurements, primarily because the passive sources are generally lower frequency than active sources—it is difficult to generate low-frequency motions with active sources. On the other hand, the receiver arrays for passive-source investigations often are not designed to capture near-surface details. In future studies, we encourage the derivation of models based on a combination of active and passive sources or a wider range of passive-array radii.

We temper our positive conclusions with the observation that although the sites are quite typical of those from which strong-motion data have been obtained in California, the sites at which the investigations were conducted are easy sites, without strong gradients of the slowness with depth (this includes both gradients over several tens of meters as well as abrupt changes between materials of very different lithology or geologic age). It would be of great interest to repeat this blind interpretation exercise at other locations with subsurface slowness variations different than those in the Santa Clara Valley of California. One such blind study was conducted by Asten *et al.* (2005) in a region with 21 m of soft silt ($S_S = 6.25$ sec/km) overlying firm glacial till ($S_S = 1.81$ sec/km); they found that the slownesses above and below the interface, as well as the depth to the interface, were within 5% of independently determined values.

Acknowledgments

We thank all participants in the blind interpretation exercise for giving freely of their tiuggesting that the first author conduct the blind interpretation exercise, Mark Goldman for vertical profiles for the selected site along the Catchings *et al.* (2006) profile, Carl Wentworth for data, discussions, and figures, Michael Asten, Dominik Lang, and Bill Stephenson for models, Tom Holzer for data, and Tom Holzer, Chuck Langston, Paco Chávez-García, Eric Thompson, and an anonymous individual for critical reviews of the manuscript. One of us (M. W. A.) was supported for acquisition of passive microtremor data at the listed sites via USGS External Grants Number 04HQGR0030 and Number 05HQGR0022, together with the loan of Program for the Array Seismic Studies of the Continental Lithosphere (PASSCAL) intermediate period seismometers and recorders from the Incorporated Research Institutions for Seismology. Seismic technicians Russell Sell and Chris Dietel provided invaluable field and data processing support.

References

Asten, M. W. (2005). An assessment of information on the shear-velocity profile at Coyote Creek, San Jose, from SPAC processing of microtremor array data, in *Blind Comparisons of Shear-Wave Velocities at Closely-Spaced Sites in San Jose, California*, M. W. Asten and D. M. Boore (Editors), *U.S. Geol. Surv. Open-File Rept. 2005-1169*, part 2, 47 pp.

Asten, M. W. (2006). On bias and noise in passive seismic data from finite circular array data processed using SPAC methods, *Geophysics* **71,** V153–V162.

Asten, M. W., and D. M. Boore (Editors) (2005a). *Blind Comparisons of Shear-Wave Velocities at Closely-Spaced Sites in San Jose, California*, *U.S. Geol. Surv. Open-File Rept. 2005-1169*.

Asten, M. W., and D. M. Boore (2005b). Comparison of shear-velocity profiles of unconsolidated sediments near the Coyote borehole (CCOC) measured with fourteen invasive and non-invasive methods, in *Blind Comparisons of Shear-Wave Velocities at Closely-Spaced Sites in San*

Jose, California, Asten, M. W., and D. M. Boore (Editors), *U.S. Geol. Surv. Open-File Rept. 2005-1169*, part 1, 35 pp.

Asten, M. W., W. R. Stephenson, and P. Davenport (2005). Shear-wave velocity profile for Holocene sediments measured from microtremor array studies, SCPT, and seismic refraction, *J. Eng. Environ. Geophys.* **10,** 235–242.

Bay, J., J. Gilbert, K. Park, and I. Sasankul (2005). Shear wave velocity profiling using spectral analysis of surface waves (SASW) at Williams Street Park & Coyote Creek Borehole San Jose, CA, in *Blind Comparisons of Shear-Wave Velocities at Closely-Spaced Sites in San Jose, California*, M. W. Asten and D. M. Boore (Editors), *U.S. Geol. Surv. Open-File Rept. 2005-1169*, part 2, 22 pp.

Boore, D. M. (2003a). A compendium of *P*- and *S*-wave velocities from surface-to-borehole logging: summary and reanalysis of previously published data and analysis of unpublished data, *U.S. Geol. Surv. Open-File Rept. 03-191*, 13 pp.

Boore, D. M. (2003b). Prediction of ground motion using the stochastic method, *Pure Appl. Geophys.* **160,** 635–676.

Boore, D. M. (2006). Determining subsurface shear-wave velocities: a review, in *Third International Symposium on the Effects of Surface Geology on Seismic Motion*, P.-Y. Bard, E. Chaljub, C. Cornou, F. Cotton and P. Gueguen (Editors), Grenoble, France, 30 August–1 September 2006, Laboratoire Central des Ponts et Chaussées, 67–85.

Boore, D. M., and G. M. Atkinson (2007). Boore–Atkinson NGA ground motion relations for the geometric mean horizontal component of peak and spectral ground motion parameters, PEER Report 2007/01, Pacific Earthquake Engineering Center, Berkeley, California.

Boore, D. M., and G. M. Atkinson (2008). Ground-motion prediction equations for the average horizontal component of PGA, PGV, and 5%-damped PSA at spectral periods between 0.01 s and 10.0 s, *Earthq. Spectra* (in press).

Boore, D. M., and L. T. Brown (1998a). Comparing shear-wave velocity profiles from inversion of surface-wave phase velocities with downhole measurements: systematic differences between the CXW method and downhole measurements at six USC strong-motion sites, *Seism. Res. Lett.* **69,** 222–229.

Boore, D. M., and L. T. Brown (1998b). Erratum to "Comparing shear-wave velocity profiles from inversion of surface-wave phase velocities with downhole measurements: systematic differences between the CXW method and downhole measurements at six USC strong-motion sites", *Seism. Res. Lett.* **69,** 406.

Boore, D. M., and W. B. Joyner (1997). Site amplifications for generic rock sites, *Bull. Seismol. Soc. Am.* **87,** 327–341.

Boore, D. M., and E. M. Thompson (2007). On using surface-source downhole-receiver logging to determine seismic slownesses, *Soil Dyn, Earthq. Eng.* **27,** 971–985.

Brown, L. T., D. M. Boore, and K. H. Stokoe (2002). Comparison of shear-wave slowness profiles at ten strong-motion sites from non-invasive SASW measurements and measurements made in boreholes, *Bull. Seismol. Soc. Am.* **92,** 3116–3133.

Building Seismic Safety Council (BSSC) (2004). NEHRP recommended provisions for seismic regulations for new buildings and other structures, part 1—provisions, part 2—commentary, Report No. FEMA 450, 2003 edition, prepared by the BSSC for the Federal Emergency Management Agency: available from BSSC at http://www.bssconline.org/ (last accessed May 2008).

Catchings, R. D., M. R. Goldman, and G. Gandhok (2006). Structure and velocities of the northeastern Santa Cruz Mountains and the western Santa Clara Valley, California, from the SCSI-LR seismic survey, *U.S. Geol. Surv. Open-File Rept. 2006-1014*, 78 pp.

Choi, Y., and J. P. Stewart (2005). Nonlinear site amplification as function of 30 m shear wave velocity, *Earthq. Spectra* **21,** 1–30.

Cornou, C., M. Ohrnberger, D. M. Boore, K. Kudo, and P.-Y. Bard (2007). Derivation of structural models from ambient vibration array recordings: results from an international blind test, in *Third International Symposium on the Effects of Surface Geology on Seismic Motion*, P.-Y. Bard, E. Chaljub, C. Cornou, F. Cotton and P. Gueguen (Editors) Grenoble, France, 30 August–1 September 2006, Laboratoire Central des Ponts et Chaussées.

Day, S. M. (1996). RMS response of a one-dimensional halfspace to *SH*, *Bull. Seismol. Soc. Am.* **96,** 363–370.

Dobry, R., R. D. Borcherdt, C. B. Crouse, I. M. Idriss, W. B. Joyner, G. R. Martin, M. S. Power, E. E. Rinne, and R. B. Seed (2000). New site coefficients and site classification system used in recent building seismic code provisions, *Earthq. Spectra* **16,** 41–67.

Hanson, R. T., M. W. Newhouse, C. M. Wentworth, C. F. Williams, T. E. Noce, and M. J. Bennett (2002). Santa Clara Valley Water District multi-aquifer monitoring-well site, Coyote Creek Outdoor Classroom, San Jose, California, *U.S. Geol. Surv. Open-File Rept. 02-369*, 4 pp.

Hartzell, S., D. Carver, T. Seiji, K. Kudo, and R. Herrmann (2005). Shallow shear-wave velocity measurements in the Santa Clara Valley; comparison of spatial autocorrelation (SPAC) and frequency wavenumber (FK) methods, in *Blind Comparisons of Shear-Wave Velocities at Closely-Spaced Sites in San Jose, California*, M. W. Asten and D. M. Boore (Editors), *U.S. Geol. Surv. Open-File Rept. 2005-1169*, part 2, 9 pp.

Hayashi, K. (2005). The result of surface wave method in the Coyote Creek borehole (Williams Park), in *Blind Comparisons of Shear-Wave Velocities at Closely-Spaced Sites in San Jose, California*, M. W. Asten and D. M. Boore (Editors), *U.S. Geol. Surv. Open-File Rept. 2005-1169*, part 2, 10 pp.

Kayen, R. (2005). The spectral analysis of surface waves measured at William Street Park, San Jose, California, using swept-sine harmonic waves, in *Blind Comparisons of Shear-Wave Velocities at Closely-Spaced Sites in San Jose, California*, M. W. Asten and D. M. Boore (Editors), *U.S. Geol. Surv. Open-File Rept. 2005-1169*, part 2, 7 pp.

Lang, D. H., and J. Schwarz (2005). Identification of the subsoil profile characteristics at the Coyote Creek Outdoor Classroom (CCOC), San José, from microtremor measurements—a contribution to the CCOC blind comparison experiment, in *Blind Comparisons of Shear-Wave Velocities at Closely-Spaced Sites in San Jose, California*, M. W. Asten and D. M. Boore (Editors), *U.S. Geol. Surv. Open-File Rept. 2005-1169*, part 2, 7 pp.

Oze, C. J., J. L. Matthew, C. M. Wentworth, R. T. Hanson, D. K. Bird, and R. G. Coleman (2003). Chromium geochemistry of serpentinous sediment in the Willow core, Santa Clara County, California, *U.S. Geol. Surv. Open-File Rept. 03-251*, 24 pp.

Newhouse, M. W., R. T. Hanson, C. M. Wentworth, R. R. Everett, C. F. Williams, J. C. Tinsley, T. E. Noce, and B. A. Carkin (2004). Geologic, water-chemistry, and hydrologic data from multiple-well monitoring sites and selected water-supply wells in the Santa Clara Valley, California, 1999—2003, *U.S. Geol. Surv. Sci, Investig. Rept. 2004-5250*, 142 pp.

Noce, T. E., and T. L. Holzer (2003). Subsurface exploration with the cone penetration testing truck, *U.S. Geol. Surv. Fact Sheet 028-03*.

Power, M., B. Chiou, N. Abrahamson, Y. Bozorgnia, T. Shantz, and C. Roblee (2008). An overview of the NGA project, *Earthq. Spectra* (in press).

Stephenson, W. J., J. N. Louie, S. Pullammanappallil, R. A. Williams, and J. K. Odum (2005). Blind shear-wave velocity comparison of ReMi and MASW results with boreholes to 200 m in Santa Clara Valley: implications for earthquake ground-motion assessment, *Bull. Seismol. Soc. Am.* **95,** 2506–2516.

Stephenson, W. J., R. A. Williams, J. K. Odum, and D. M. Worley (2005). Comparison of ReMi, and MASW shear-wave velocity techniques with the CCOC borehole to 100 m, Santa Clara Valley, in *Blind Comparisons of Shear-Wave Velocities at Closely-Spaced Sites in San Jose, California*, M. W. Asten and D. M. Boore (Editors), *U.S. Geol. Surv. Open-File Rept, 2005-1169*, part 2, 6 pp.

Wentworth, C. M., and J. C. Tinsley (2005). Geologic setting, stratigraphy, and detailed velocity structure of the Coyote Creek borehole, Santa

Clara valley, California, in *Blind Comparisons of Shear-Wave Velocities at Closely-Spaced Sites in San Jose, California*, M. W. Asten and D. M. Boore (Editors), *U.S. Geol. Surv. Open-File Rept. 2005-1169*, part 2, 26 pp.

Williams, R. A., W. J. Stephenson, J. K. Odum, and D. M. Worley (2005). *P*- and *S*-wave seismic reflection and refraction measurements at CCOC, in *Blind Comparisons of Shear-Wave Velocities at Closely-Spaced Sites in San Jose, California*, M. W. Asten and D. M. Boore (Editors), *U.S. Geol, Surv. Open-File Rept. 2005-1169*, part 2, 17 pp.

Yoon, S., and G. J. Rix (2005). Active and passive surface wave measurements at the William Street Park Site, using F-K methods, in *Blind Comparisons of Shear-Wave Velocities at Closely-Spaced Sites in San Jose, California*, M. W. Asten and D. M. Boore (Editors), *U.S. Geol. Surv. Open-File Rept. 2005-1169*, part 2, 15 pp.

U.S. Geological Survey
MS 977
345 Middlefield Road
Menlo Park, California 94025
boore@usgs.gov
(D.M.B.)

Centre for Environmental and Geotechnical Applications of Surface Waves (CEGAS)
School of Geosciences
Monash University
Melbourne, Victoria 3800, Australia
(M.W.A.)

Manuscript received 5 November 2007